ADSORPTION OF GOLD ATOMS ON ANATASE TiO_2(100)-1×1 SURFACE

A THESIS SUBMITTED TO
THE GRADUATE SCHOOL OF NATURAL AND APPLIED SCIENCES
OF
MIDDLE EAST TECHNICAL UNIVERSITY

BY

KIVILCIM BAŞAK VURAL

IN PARTIAL FULFILLMENT OF THE REQUIREMENTS
FOR
THE DEGREE OF MASTER OF SCIENCE
IN
PHYSICS

SEPTEMBER 2009

Approval of the thesis

ADSORPTION OF GOLD ATOMS ON ANATASE TiO_2(100)-1×1 SURFACE

Submitted by **KIVILCIM BAŞAK VURAL** in partial fulfillment of the requirements for the degree of **Master of Science in Physics Department, Middle East Technical University**, by

Prof. Dr. Canan Özgen
Dean, Graduate School of **Natural and Applied Sciences** _____

Prof. Dr. Sinan Bilikmen
Head of Department, **Physics** _____

Prof. Dr. Şinasi Ellialtıoğlu
Supervisor, **Physics Dept., METU** _____

Examining Committee Members:

Prof. Dr. Şenay Katırcıoğlu
Physics Dept., METU _____

Prof. Dr. Şinasi Ellialtıoğlu
Physics Dept., METU _____

Prof. Dr. Mehmet Çakmak
Physics Dept., Gazi U. _____

Assoc. Prof. Dr. Ersen Mete
Physics Dept., Balıkesir U. _____

Assist. Prof. Dr. Hande Toffoli
Physics Dept., METU _____

Date: _____

I hereby declare that all information in this document has been obtained and presented in accordance with academic rules and ethical conduct. I also declare that, as required by these rules and conduct, I have fully cited and referenced all material and results that are not original to this work.

Name, Last Name : Kıvılcım Başak Vural
Signature :

ABSTRACT

ADSORPTION OF GOLD ATOMS ON ANATASE TiO_2(100)-1×1 SURFACE

VURAL, KIVILCIM BAŞAK

M.S., Department of Physics

Supervisor: Prof. Dr. Şinasi Ellialtıoğlu

September 2009, 50 pages

In this work the electronic and structural properties of anatase TiO_2 (100) surface and gold adsorption have been investigated by using the first-principles calculations based on density functional theory (DFT). TiO_2 is a wide band-gap material and to this effects it finds numerous applications in technology such as, cleaning of water, self-cleaning, coating, solar cells and so on.

Primarily, the relation between the surface energy of the anatase (100)-1×1 phase and the TiO_2-layers is examined. After an appropriate atomic layer has been chosen according to the stationary state of the TiO_2 slab, the adsorption behavior of the Au atom and in the different combinations are searched for both the surface and the surface which is supported by a single Au atom/atoms. It has been observed that a single Au atom tends to adsorb to the surface which has an impurity of Au atom or atoms. Although, the high metal concentration on the surface have increased the strength of the adsorption, it is indicated that the system gains a metallic property which is believed to cause problems in the applications. In addition, the gold clusters of the dimer (Au_2) and the trimer

(Au_3) have been adsorbed on the surface and their behavior on the surface is investigate. It is observed that the interaction between Au atoms in the atomic cluster each other is stronger than that of gold clusters and the surface.

Keywords: First principle calculations, density functional theory, titanium dioxide, anatase, (100) surface reconstruction, gold clusters, solar cells.

ÖZ

ALTIN ATOMLARININ ANATAZ TiO_2(100)-1×1 YÜZEYLERİNE TUTUNMASI

VURAL, KIVILCIM BAŞAK

Yüksek Lisans, Fizik Bölümü

Tez Yöneticisi: Prof. Dr. Şinasi Ellialtıoğlu

Eylül 2009, 50 sayfa

Bu çalışmada, anatase (100) yüzeyini ve altın atomlarının bu yüzeye tutunmasının elektronik ve yapısal özellikleri yoğunluk fonksiyonu kuramına dayalı ilk prensipler hesapları kullanılarak incelendi. Titanya geniş band-aralıklı olma özelliğine sahip bir malzemedir ve bu özelliği ile suyun temizlenmesi, kendi kendini temeizleyen, kaplama, ve güneş pilleri gibi teknolojide geniş kullanım alanları bulur.

Öncelikle, anatase (100)-1×1 yüzey enerjisi ile TiO_2 katmanları arasındaki ilişki incelandi. TiO_2 tabakasının kararlılığına göre uygun atomik katman seçildikten sonra, yüzeyde ve tek Au atom/atomları ile zenginleştirilmiş yüzeyde Au atomunun tutunma davranışları ve farklı kombinasyonları araştırıldı. Tek altın atomunun Au atom/atomları safsızlığına sahip yüzeyde tutunma eğiliminde olduğu gözlendi. Yüzeydeki metal konsantrasyonun tutunmanın gücünü artırmasına rağmen, sistemin bu durumdan kaynaklı olarak uygulamalardaki problemin nedeni olduğuna inanılan metalik özellik kazandı. Ek olarak, ikili (Au_2) ve üçlü (Au_3) altın öbekleri yüzeye tutturuldu ve onların sistem içindeki davranışları

incelendi. Atomik salkım içindeki Au atomlarının birbirleriyle etkileşmesinin Au öbeklerinin yüzey ile etkileşmesinden daha güçlü olduğu gözlendi.

Anahtar Kelimeler: İlk prensip hesaplamalar, yoğunluk fonksiyonu teorisi, titanyum dioksit, anataz, (100) yüzeyi yeniden-yapılanması, altın öbekleri, güneş pili.

To my family

ACKNOWLEDGMENTS

I would like to express my deep and sincere gratitude to my supervisor Prof. Dr. Şinasi Ellialtıoğlu, for his guidance, eternal patience, and encouragement, to Prof. Dr. Mehmet Çakmak, for his computer support and advice, to Assist. Prof. Dr. Hande Toffoli and Assoc. Prof. Dr. Ersen Mete, to their critical comments, valuable information and in many others.

I also would like to thank deeply to my dear colleagues Murat Mesta, Ceren Sibel Sayın, Ceren Taylan, and Engin Torun for their cooperation and supportive discussions that were crucial for this thesis, to my special friends Mehtap Özbey, for her helpful and support motivating that were significant for me. Also, I am thankful to my physics mates.

I want to thank to best friends Pınar İçemer, Pınar Yağcı, and Duygu Sürücüoğlu, for their support in every way that was fundamental for my life. I want to thank for Canan Erden who was on my side in every time.

This work is financially supported by TÜBİTAK, The Scientific and Technological Research Council of Turkey (Grand no: TBAG-107T560).

TABLE OF CONTENTS

LIST OF TABLES

TABLES

LIST OF FIGURES

FIGURES

CHAPTER 1

INTRODUCTION

Nanoscience and nanotechnology are studied in several disciplines such as physics, material science, chemistry, biology, chemical engineering, medicine, etc. For that reason, recently rate of research activities in nanoscience and nanotechnology have increased drastically. For instance, mechanical, electrical, optical and chemical properties of a material are greatly altered with reductions in size, namely because of quantum size effect. When the materials are considered in the nanoscale, they can exhibit very different properties compared to what they exhibit on a macroscale. For example, although gold is chemically an inactive material in macroscale, it can be considered as a potential chemical catalyst at the nanoscale.

The surfaces of transition metal oxides are investigated to better understand their physical properties and it became already an important discipline.

Titanium dioxide, TiO_2, is a material of increasing scientific interest especially in surface science because of its flat and stable surfaces and because of various charge states that Ti ions can have [1]. This enables it to be an important candidate used in a wide range of applications. TiO_2 has been used in several environment-friendly applications for different purposes due to its photocatalytic property such as a photocatalist in production of hydrogen from water, cleaning of water, self-cleaning, coating, solar cells, and so on [2].

Catalysis is an important topic in surface physics for useful reactions to occur with a little help from the environment. Heterogeneous catalysis, which is one

type of catalysis, is composed of small metal clusters that are supported on an oxide surface and they enter the reaction and after the products are obtained they leave the reaction. Many growth studies of metals have been performed on reducible transition metal oxides such as TiO_2. Gold had been regarded as poorly active in a catalysis process due to its high ionization potential of 9.2 eV. Similarly, TiO_2 is not an active catalyst for CO oxidation. However, Haruta [3,4] has showed that TiO_2 supported Au has extraordinary catalysis properties even for the oxidation of CO. The structure sensitivity of CO oxidation on TiO_2 surfaces which are deposited by gold clusters is related to the size of these metal clusters due to quantum size effect [5,6]. Catalysis strongly depends on large surface to volume ratio [7] and also, preparation method, gold concentration as well as the choice of support [8].

TiO_2 is also a photocatalyst material under the ultraviolet illumination (UV). In 1972, Fujishima and Honda have discovered the decomposition of water on TiO_2 electrodes as being the catalyst [9]. In the photocatalyst system, the molecule which is induced by photon reacts with the catalyst surface. The main process of photocatalysis includes the adsorption of molecule on the surface which is subjected to a catalyzed photoreaction and/or photoexcitation. It occurs on the catalyst substrate where an electron transition or energy transfer from the ground state of molecule takes place. In the electron transfer process, the electron–hole pairs are produced via the electron jumping from occupied state to unoccupied state. If the transferred charge can be trapped, the photoexcited electron–hole pairs occur more efficiently. Because, the lifetime of the separated electrons and the corresponding holes increases due to the charge trapping which, is the most effective way to achieve by addition of the metals to the semiconducting surfaces. In other words, after excited electrons move to the metal and the hole is diffused through the semiconductor surface in which the oxidation of space can occur [10].

Photovoltaic cells/solar cells are the devices which convert the sunlight to the electric power by photovoltaic effect. In principle, electrons are excited

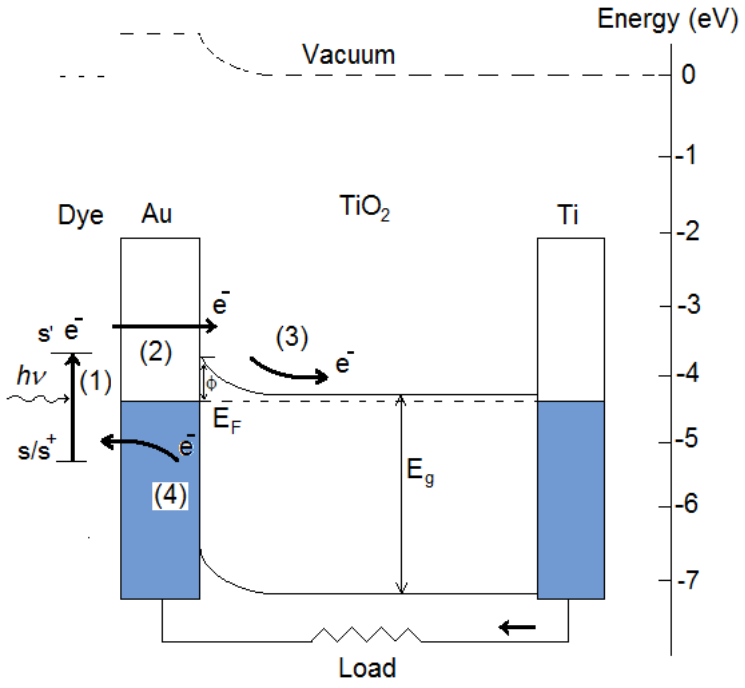

Figure 1.1: Photovoltaic device by McFarland and Tang [12]. Photon adsorption causes the electron excitation from ground state s to excited state s′ (1). Electron travels from s′ to the conducting surface layer and over the potential barrier (2), into the semiconductor (3), reaching to the ohmic back conduct (4), after reduction of the oxide holes. The Schottky barrier ϕ and Fermi energy E_F are indicated in the figure.

from the valence band to the conduction band by the light adsorption in a semiconductor, which creates electron–hole pairs. The positive holes which exist at the surface of the semiconductor electrode are utilized in oxidation. The negative charge which enters the counter-electrode leads to hydrogen after reduction. The main problem in this device is that water could not be decomposed into its constituents directly by visible light absorption, whereas TiO_2 absorbs only ultraviolet portion of the solar emission due to its large band gap (∼3.2 eV). Therefore, the efficiency of solar energy conversion is very low due to this property. But the width of the band gap is an indicator of the chemical bond strength which can be commonly thought as an advantage

for this application. This dilemma was solved by using an electron transfer sensitizer absorbing in the visible light to inject the charge carriers across the semiconductor–electrolyte junction into a substrate with a suitable band gap [11]. Cost-effective photovoltaic devices are being still studied by many scientist in different disciplines. One of these studies was done by McFarland and Tang [12]. Their device has been fabricated recently as an $Au/TiO_2/Ti$ multilayer structure (Fig. 1.1). In principle, this device structure in which the light absorption is done by the deposited dye molecules on the surface of an ultrathin metal–semiconductor junction of the Schottky diode. Afterwards, photoexcited electrons which travel over the Schottky barrier produce the photocurrent. The efficiency of the device which was used by McFarland and Tang was pointed out as the long ballistic path length of the low-energy electrons in the noble metals since it allows a large fraction of the trapped electrons. Hence, this device could work via charge separation and majority charge transport. In that work, the Schottky barrier is a potential barrier between TiO_2 and gold layers which created the local electrostatic field. Therefore, it is important that the interaction between TiO_2 surface and Au atom particles should be investigated at nanoscale regime to reach higher efficiency in various applications.

In nature, titania mainly exists in three different crystal structures, which are anatase, rutile, and brookite. The applications of brookite is not yet sufficiently known. One of the main reasons that is not popular enough is its complex structure since this property gives rise to additional difficulties in crystal growth [13]. For that reason, anatase and rutile are the most widely used modifications of titania. Thermodynamically, rutile is more stable than anatase structure that is why some experimental problems can arise during the growth process of a single crystal anatase. As a result, rutile structure, particulary its most stable (110) face, has been widely investigated in the surface science discipline. On the other hand, TiO_2 nanoparticles are commonly in anatase form with (101) and (100) facets and to this end anatase surfaces are generally used in photocatalytic application due to their higher (photo)catalytic activity [14,15]. These polytype

surfaces, (100) and (101), have experimentally been reconstructed to a 1×1 and 1×n termination, respectively [16,17]. In addition, to these anatase with (001) surface shows high photocatalytic activity in decomposition of water molecule [18].

In this thesis, we have investigated the structural and electronic properties of Au atom/atoms adsorption on TiO_2 anatase (100)-1×1 surface by using Density Functional Theory. The theoretical background of this work is briefly discussed in Chapter 2. DFT has been widely used "ab initio" method by researchers from chemistry, physics, and from other disciplines. We only have discussed the main points about this theory and its relation to this thesis, as it is used in the calculations.

The structural and electronic properties of adsorption of Au atom/atoms on TiO_2 have been discussed in Chapter 3. This chapter contains four parts: (1) details of the calculations and discussion of the TiO_2 anatase (100)-1×1 surface, (2) adsorption of a single Au atom on both the clean and unclean surfaces, (3) adsorption of Au dimer (Au_2) on the bare surface and (4) of Au trimer (Au_3).

Finally, the conclusion of this study is presented in Chapter 4.

CHAPTER 2

THEORETICAL BACKGROUND

In this chapter, the theoretical approximations and approaches used in Density Functional Theory (DFT) based methods will be presented [19,20].

2.1 The problem of structure of matter

It is a complex problem to describe the physical and chemical properties of matter at the microscopic scale. In general, we handle a collection of interacting atoms, which may also be affected by some external field. This ensemble of particles may be in the gas phase (molecules and clusters) or in a condensed phase (solids, surface, wires). However, in any case the system can be described as a set of atomic nuclei and electrons interacting though electrostatic force. Therefore, the Hamiltonian of such a system can be written in the following general form:

$$H = H_{el} + H_{nucl} \tag{2.1}$$

where

$$H_{el} = -\sum_{i=1}^{N} \frac{\hbar^2}{2m}\nabla_i^2 + \frac{e^2}{8\pi\epsilon_0}\sum_{i=1}^{N}\sum_{j\neq i}^{N}\frac{1}{|\mathbf{r}_i - \mathbf{r}_j|} - \frac{e^2}{4\pi\epsilon_0}\sum_{I=1}^{P}\sum_{i=1}^{N}\frac{Z_I}{|\mathbf{R}_I - \mathbf{r}_i|} \tag{2.2}$$

$$H_{nucl} = -\sum_{I=1}^{P} \frac{\hbar^2}{2M_I}\nabla_I^2 + \frac{e^2}{8\pi\epsilon_0}\sum_{I=1}^{P}\sum_{J\neq I}^{P}\frac{Z_I Z_J}{|\mathbf{R}_I - \mathbf{R}_J|} \tag{2.3}$$

where $\mathbf{r}_i$, $(i = 1, ..., N)$ is a set of N electron coordinates and $\mathbf{R}_I$, $(I = 1, ..., P)$ is a set of P nuclear coordinates. The factor of $\frac{1}{2}$ has been included in order to avoid double counting of terms in the series representation.

In principles, all the properties can be derived by solving the time independent many-body Schrödinger equation;

$$H\Psi_n(\mathbf{R}, \mathbf{r}) = \varepsilon_n \Psi_n(\mathbf{R}, \mathbf{r}) \tag{2.4}$$

where ε_n are energy eigenvalues and $\Psi_n(\mathbf{R}, \mathbf{r})$ are the corresponding eigenstates or wave functions, which must be antisymmetric with respect to exchange of electronic coordinates in r, since electrons are fermions. Nuclei of the same species also obey according to the same rule because of their nuclear spin, so that eigenstate or wave function must be symmetric or antisymmetric with respect to exchange of nuclear variables in R.

2.2 Adiabatic Approximation

The motivation behind the Born–Oppenheimer approximation [19] is that the motion of the electrons is usually much faster than the motion of the nuclei. In fact the smaller mass of the electrons as compared to that of the protons is 1/1836 which means that their velocity is much larger.

Within the adiabatic approximation, the possibility having of a non-radiative transition between different electronic eigenstates are ignored. Transition can only arise through coupling with an external electromagnetic field and involve the solution of the time-dependent and Schrödinger equation. Under these conditions, full wave function can be written as;

$$\Psi(\mathbf{R}, \mathbf{r}, t) = \sum_m \Theta_m(\mathbf{R}, t)\Phi_m(\mathbf{R}, \mathbf{r}) \tag{2.5}$$

where $\Theta_m(\mathbf{R}, t)$ is nuclear wave function, $\Phi_m(\mathbf{R}, \mathbf{r})$ is the electronic wave function So, separation of variables leads to, for the electrons as,

$$[\hat{T}_e + \hat{V}_{ee} + \hat{V}_{en}]\Phi_m(\mathbf{R}, \mathbf{r}) = \varepsilon_m \Phi_m(\mathbf{R}, \mathbf{r}) \tag{2.6}$$

and for the nuclei as

$$[\hat{T}_n + \hat{V}_{nn} + \varepsilon(\mathbf{R})]\Theta_m(\mathbf{R}, t) = \varepsilon_m \Theta(\mathbf{R}, t)_m. \tag{2.7}$$

In practice within the adiabatic approximation most of the applications are in the ground state ($m = 0$)

$$[\hat{T}_e + \hat{V}_{ee} + \hat{V}_{en}]\Phi_0(\mathbf{R}, r) = \varepsilon_0 \Phi_0(\mathbf{R}, \mathbf{r}) \tag{2.8}$$

$$[\hat{T}_n + \hat{V}_{nn} + \varepsilon(\mathbf{R})]\Theta_0(\mathbf{R}, t) = \varepsilon_0 \Theta_0(\mathbf{R}, t) \tag{2.9}$$

2.3 Pre–Density Functional Theory

2.3.1 Hartree and Hartree–Fock approximation

The main problem in the structure of matter is to solve the Schrödinger equation of a many-particle system in the external Coulombic field created by a collection of atomic nuclei. The exact solution is possible only in the case of the uniform electron gas, for atoms with a small number of electrons or a few small molecules. In order to achieve this, approximations one in order. The first approximation to solve the many-body problem was proposed by Hartree [21], which is a variational wave function based approach. The basic assumption of it is a simple product of single-particle, although it is used a many-particle technique. In the Hartree approximation, the electrons are considered as occupying single particle orbitals which are determine the wave function. Each electron feels the electrostatic field which was due to the central potential of the nucleus together with the field created by the other electrons. In this case, approximate wave function can be obtained from the variational principle,

$$\Phi(\mathbf{x}_1, \mathbf{x}_2, \ldots, \mathbf{x}_N) = \phi_1(\mathbf{x}_1)\phi_2(\mathbf{x}_2)\ldots\phi_N(\mathbf{x}_N) \tag{2.10}$$

and the one-particle Schrödinger equation proposed by Hartree is,

$$\left(-\frac{\hbar^2}{2m}\nabla^2 + V_{ext}(\mathbf{R}, \mathbf{r}) + \int \frac{\sum_{j\neq i}^{N} |\phi_j(\mathbf{r}')|^2}{|\mathbf{r} - \mathbf{r}'|} d\mathbf{r}'\right)\phi_i(\mathbf{r}) = \varepsilon_i \phi_i(\mathbf{r}) \tag{2.11}$$

where the third term on the left hand side is the classical electrostatic potential due to the charge distribution of all the other electrons. The Hartree term is that the energy of the many-body system is sum of the eigenvalues of equation (2.11). However, the electron-electron interaction is counted twice in this equation. So, the correct expression for the Hartree energy can be written as,

$$E^H = \sum_{i=1}^{N} \varepsilon_i - \frac{1}{2} \int \int \frac{\rho_i(\mathbf{r})\rho_j(\mathbf{j})}{|\mathbf{r}_i - \mathbf{r}_j|} d\mathbf{r}_i d\mathbf{r}_j \ . \tag{2.12}$$

The problem of Hartree approximation is such that it does take the electrons as distinguishable particles, However electrons are indistinguishable spin-$\frac{1}{2}$ particles and the obey Pauli exclusion principle. If two electrons are exchange, the wave function must change sign. Thus, a Slater determinant is formed from the one–particle orbitals in order to achieve the correct antisymmetric wavefunction [22],

$$\Phi_{HF}(x_1, x_2, \ldots, x_N) = \frac{1}{\sqrt{N!}} \begin{vmatrix} \phi_1(1) & \phi_2(1) & \cdots & \phi_N(1) \\ \phi_1(2) & \phi_2(2) & \cdots & \phi_N(2) \\ \vdots & \vdots & \ddots & \vdots \\ \phi_1(N) & \phi_2(N) & \cdots & \phi_N(N) \end{vmatrix} \tag{2.13}$$

$$\Phi_{HF} = \frac{1}{\sqrt{N!}} \sum_{i=1}^{N} (-1)^{P(i)} \phi_{i1}(\mathbf{x}_1)\phi_{i2}(\mathbf{x}_2) \ldots \phi_{iN}(\mathbf{x}_N) \tag{2.14}$$

where $P(i)$ is mathematical properties of determinant expression and i refers to N indices. This wave function allows particle exchange in the correct manner. The approximation consists of the wave function in the form (2.14) is called Hartree–Fock (HF) or self consistent field (SCF) model. HF equation provides good description of inter-atomic bonding but many-body correlations are completely ignored.

2.3.2 Thomas–Fermi Theory

Thomas and Fermi, independently of each other, gave a perspective for constructing the total energy in terms of the electronic density without using to one-electron orbitals [23]. They proposed the expression for the kinetic, exchange, and correlation energies of the homogenous electron gas to construct the same quantities for the inhomogenous system as; $E_\alpha[\rho] = \int \rho(\mathbf{r})\varepsilon_\alpha[\rho(\mathbf{r})]d\mathbf{r}$ where $\varepsilon_\alpha[\rho(\mathbf{r})]$ is the energy, a functional of density of corresponding to calculated locally at the value assumed by the density a function of space α. This idea was the first time that the locally density functional approximation (LDA) was used. The relationship between the Fermi energy and density for homogenous electron gas is given by;

$$\rho = \frac{1}{3\pi^2}\left(\frac{2m}{\hbar^2}\right)^{3/2}\epsilon_F^{3/2} \tag{2.15}$$

and the kinetic energy of homogenous gas is $T = 3\rho\epsilon_F/5$. When it is used with electron density formula, the kinetic energy density formulation can be derived similarly. Finally, total energy expression without exchange and correlation can be obtain in Thomas–Fermi theory as,

$$E_{TF}[\rho] = C_k \int \rho(\mathbf{r})^{5/3}d\mathbf{r} + \int \rho(\mathbf{r})v_{ext}(\mathbf{r})d\mathbf{r} + \frac{1}{2}\int\int \frac{\rho(\mathbf{r})\rho(\mathbf{r}')}{|\mathbf{r}-\mathbf{r}'|}d\mathbf{r}d\mathbf{r}' \tag{2.16}$$

where $C_k = 3(3\pi^2)^{2/3}/10 = 2.871$ atomic units which is coming from kinetic energy term. Thomas–Fermi theory does not have the exchange and correlation effects and Hartree equation described the ground states even better than that. However, it contains the fundamental ideas necessary for the development Density Functional Theory.

2.4 Modern Density Functional Theory

The main theorems were reported first by Hohenberg–Kohn (HK) in 1964 [24], and they were reformulated by Kohn–Sham in 1965 [25]

2.4.1 Hohenberg–Kohn Theory

The energy can be written in terms of the electron density in the Thomas–Fermi approximation. Hohenberg and Kohn have proven a theorem on mathematical ground which confirms the Thomas–Fermi idea. The theorem is divided into two parts.

1. For any system of interacting particles of the ground state energy is a unique functional of the particle density, $E_0 = E[\rho(\mathbf{r})]$. There cannot be two different external potentials $\upsilon(\mathbf{r}) \neq \upsilon'(\mathbf{r})$ that correspond to the same electronic density for the ground state.

2. The minimum value of the functional $E = E[\rho(\mathbf{r})]$ for the energy can be define by variations $\delta\rho(\mathbf{r})$ of the particle density at equilibrium density $\rho_0(\mathbf{r})$,

$$E = E[\rho_0(\mathbf{r})] = \min\{E[\rho(\mathbf{r})]\} \tag{2.17}$$

2.4.2 Self-consistent Kohn–Sham equations

Hartree term refers to the classical electrostatic energy, which is known exactly for the electron-electron problem. However, it is a problem that the kinetic energy $T =< \Phi|\hat{T}|\Phi >$ expression is written in terms of the electronic density. Non-interacting electrons are described by an antisymmetric wave function of the Slater determinant, made of one-electron orbitals in Hartree–Fock theory. According to the idea of Kohn and Sham, when non-interacting electrons in a system create the same electronic density as the interacting system, the kinetic energy of the interacting system can be calculated similarly. In other words, the kinetic energy of the interacting electrons is written by that of the non-interacting system and the correlation part added. The Kohn–Sham can be expressed as,

$$E_{KS}[\rho] = T_R[\rho] + \int \rho(\mathbf{r})\upsilon_{ext}(\mathbf{r})d\mathbf{r} + \frac{1}{2}\int\int \frac{\rho(\mathbf{r})\rho(\mathbf{r}')}{|\mathbf{r}-\mathbf{r}'|}d\mathbf{r}d\mathbf{r}' + E_{XC}[\rho] \tag{2.18}$$

where density is determined expression, $\rho(\mathbf{r}) = \Sigma_{i=1}^{N_s}|\varphi_i(\mathbf{r})|^2$, and $E_{XC}[\rho]$ is the exchange-correlation functional. The energy functional has been expressed

in terms of the KS orbitals (N_s) by this formula, which minimize the non-interacting electronic kinetic energy under the fixed density constraint. Although, Kohn–Sham orbitals do not have a clear meaning by themselves, they can be described the one-electron orbitals or single-particle eigenstate.

2.5 Functionals for Exchange and Correlation

The exchange energy (E_X), and correlation energy terms (E_C) are not known in explicit form in DFT. The approximation here is that the sum of the two terms E_X+E_C is the meaningful quantity. This two terms are approximated relativity more or less accurately which is depend on the E_{XC} functional. In the exchange and correlation functionals approximations, the main idea is to reach the point where both terms are treated in a similar manner.

2.5.1 The Local Density Approximation (LDA)

The local density approximation [26] or in magnetic system local spin density approximation (LSDA) has been the most widely used approximation to calculate the exchange–correlation energy for time. The main idea is to assume generally an electronic system as locally homogenous, for which the exchange–correlation hole corresponds to the homogenous gas. In practice, the exchange–correlation terms in the local density is an integral over all space and the exchange–correlation energy can be obtained in density at each point in the volume.

$$E_{XC}^{LDA}[\rho] = \int \rho(\mathbf{r})\epsilon_{XC}^{LDA}[\rho(\mathbf{r})]d\mathbf{r} \tag{2.19}$$

where,$\epsilon_{XC}^{LDA}$is exchange-correlation energy density of the system and its value is in terms of the exchange–correlation hole,

$$\epsilon_{XC}^{LDA}[\rho] = \frac{1}{2}\int \frac{\rho_{XC}^{LDA}(\mathbf{r},\mathbf{r}')}{|\mathbf{r}-\mathbf{r}'|}d\mathbf{r}'. \tag{2.20}$$

L(S)DA works the best for solids close to homogenous gas. However, it works well for inhomogenous cases due to certain reasons:

1. It can identify homogenous system well.

2. It gives an overestimated the binding energy of molecule and cohesive energy of solids.

3. The geometries of systems involving strong bonds (covalent, ionic, and metallic) are described good within the LDA

4. But, the description of systems involving weak bonds (hydrogen or van der Walls) fail within the LDA

5. Chemical trends such as ionization potential are usually correct.

Although L(S)DA is very successful approximation for many systems such as; bulk metal, semiconductors, and ionic crystals, it is known to fail to reproduce due to its number of attributes. Some important of them;

i) Electronic densities of atoms in the core region are poor because LDA fails to cancel the self-interaction.

ii) Non-local correlation effect is not taken into account inherently by the LDA.

iii) The energy band gap within LDA is smaller than the true band gap.

iv) Strongly correlated systems such as transition metal oxides are poorly characterized by LDA.

2.5.2 Generalized Gradient Approximation (GGA)

The matter of electronic density of inhomogenous systems are carried out with an expansion of the density in terms of the gradient and higher order derivatives. In general, the exchange–correlation energy in basic form can be written as;

$$E_{XC}[\rho] = \int \rho(\mathbf{r})\varepsilon_{XC}[\rho(\mathbf{r})]d\mathbf{r} + \int F_{XC}[\rho(\mathbf{r}), \nabla\rho(\mathbf{r}), \nabla^2\rho(\mathbf{r}), \ldots]d\mathbf{r} \qquad (2.21)$$

where the function F_{XC} that modifies the LDA expression relative to the variation of the density. Naturally, all the formal properties cannot be enforced at the same time. Numerous forms for F_{XC} have been proposed by Langreth–Mehl, Becke–Lee–Yang–Parr (BLYP), Perdew–Wang (PW91), and Perdew–Burke–Enzerhof (PBE). We only explained here our choice, namely the PBE functional

in the calculations.

PBE functional

Perdew, Burke, and Enzerhof (PBE) [27] functional approximation can propose to solve one problem in the GGAs. It is originated from that the reduced to the second order gradient expansion for density variations are small. The result of this case, the linear response of a uniform gas is described with GGAs less satisfactory than L(S)DA.

The general trends of GGAs concerning improvements over the LDA are following:

1. They enhance binding and atomic energies.

2. They improve bond lengths and angles.

3. They improve energetics, geometries, and dynamical properties of water, ice, and water clusters. Especially, BLYP and PBE show best agreement with experimental results in terms of these. In general, although, they are not clear the description of F–H bond, this improves for the case of hydrogen-bounded systems.

4. Semiconductors are marginally better described within the LDA than in GGA, except for the binding energies.

5. For the 4d–5d transition metals the improvement of the GGA over the LDA is not clear.

6. Lattice constant of noble metals (Au, Ag, Pt) are overestimated in GGA, while they are closer to the experimental results in LDA.

2.6 Pseudopotentials

The concept of "pseudopotential" in electronic structure is related to the replacement of the strong Coulomb potential due to the nucleus, on the effects of the tightly bound core electrons, by an effective ionic potential acting on the valence electron. In other words, a pseudopotential is used to compute prop-

erties of valence electron due to unchanged core electron states into different chemical environments and makes use of the valence wave functions orthogonality to the core states. The pseudopotential process to be reproduced starts within independent-particle approximation, just like in the Kohn–Sham density functional approach. The valence states are seen to oscillate rapidly in the region occupied by the core electrons because of the strong ionic potential in this region. These oscillations sustain the orthogonality between the core and valence states due to Pauli exclusion principle. The valence state generated from pseudopotential construction leads to smoother pseudo-function because the resulting potential is a much weaker one than the original potential.

Pseudopotential calculations are based upon "*ab initio*" norm-conserving potentials in the most modern applications. Pseudopotentials require "norm-conserving" property in order to provide accurate and transferable potential, which provides that although the valence properties are defined in different environments such as atoms, molecules, and ions, they can be rightly described by pseudopotential constructed in one environment. We presented two of many different types of approximations in order to create smooth, transferrable, and accurate pseudofunctions in this subsection.

2.6.1 Ultrasoft Pseudopotential

One approach is known as "ultrasoft pseudopotentials" [28] which provides accurate calculations by transformation that rewrites the non-local potential in a form involving a smooth and an auxiliary function around each ion core having the rapidly varying part of the densities. Thus, the smaller the planewave cut-off, the smaller the number of planewaves that is required by this way. Smooth functions that represent each atomic state are the solution of the generalized eigenvalue problem.

2.6.2 Projector Augmented Waves

The projector augmented wave (PAW) [29] method is a general approach to a solution of electronic problem that reformulates the formal simplicity of the traditional plane-wave pseudopotential approach, adapting it to modern techniques for calculation of the total energy, forces, and stress. It introduces projectors and auxiliary localized functions similar to the ultrasoft pseudopotential method. Also, the total energy is described a functional in the PAW approach and it uses advanced algorithms for efficient solutions of the generalized eigenvalue problem. However, calculations in the PAW approach based on all-electron wavefunctions, so it recovers the wavefunction with the core region of atoms as well. Hence, this method can be incorporated into existing pseudopotential codes with relatively minor additional effort.

2.7 Numerical Calculations

We have used Vienna *Ab-initio* Simulation Package (VASP) for our *ab initio* calculations [30,31]. VASP allows the electronic structure of the system with periodic boundary conditions to be calculated using ultrasoft Vanderbilt pseudopotentials, or the Projected Augmented Wave method, and a plane wave basis set. All calculations are performed within the DFT formalism.

CHAPTER 3

GOLD CLUSTERS ON ANATASE (100) SURFACE

3.1 Computational Details

First principle total energy calculations have been carried out within density functional theory (DFT) via plane-wave basis sets and the projector augmented wave (PAW) potential [29]. The exchange–correlation effects have been calculated with the Perdew–Buke–Ernzerhof (PBE) [27] functional of the generalized gradient approximation (GGA). The Brillouin zone (BZ) integrations have been carried out using the Monkhorst–Pack scheme [32]. During the investigation of Monkhorst–Pack scheme, the tolerance for energy convergence was taken to be 10^{-3} eV for the anatase bulk calculation and 10^{-2} eV for anatase (100)-1×1 surface calculation. As a result, 6×6×1 k-point mesh was decided as suitable for our anatase (100)-1×1 surface calculations. The lattice parameters of anatase TiO_2 bulk were calculated to be a=b=3.833 Å, c=9.727 Å and a $D_{4h}^{19}(I4_1/amd)$ space-group symmetry was used for tetragonal structure. These values were 1% higher that the experimental results reported as a=b=3.785 Å, c=9.514 Å [33]. These lattice parameters were used to construct periodic slabs for the (100) surface. While surface relaxation was done, the convergence tolerance for energy was taken to be 10^{-4} eV and the force on each of unconstrained atoms was less than 0.05 eV/Å, except on those bonded to the atoms in fixed layer.

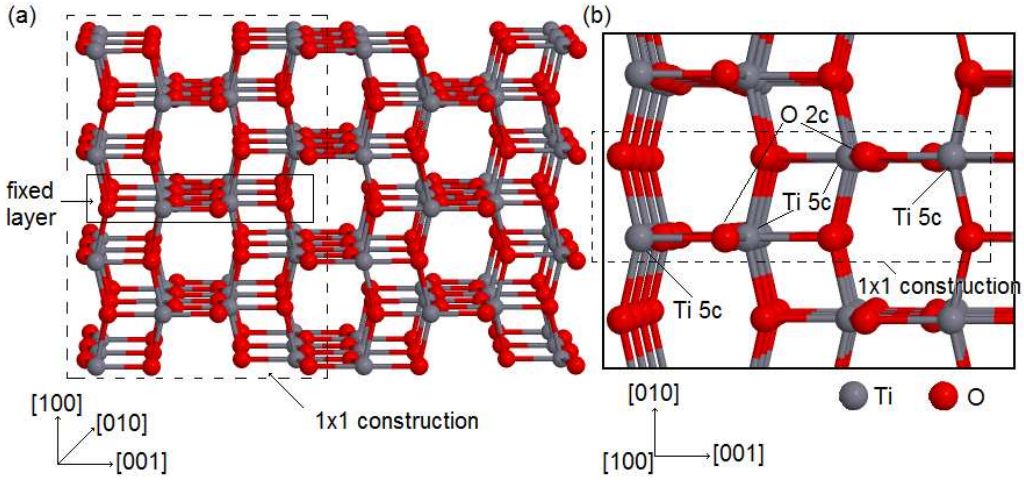

Figure 3.1: Front (a) and top (b) views of the slab modeling the anatase (100) surface. A 1×1 unit slab and a unit cell are indicated by the dash rectangles in (a) and (b), respectively.

The cutoff energy used was 400 eV. For the Ti, O, and Au pseudopotentials, d^3s^1, s^2p^4, and s^1d^{10} electronic configurations have been adopted, respectively. The charge analysis was done by using the Bader method [45,46,47].

3.2 Results and Discussions

3.2.1 Anatase (100) clean surface

The relaxed structure of the clean (100) TiO_2 anatase surface is presented in this subsection. A supercell with the dimensions of 3.83×9.73×28.75 Å^3 includes 1×1 unit in the surface plane and the vacuum region is taken as ∼14 Å. Previous theoretical studies have shown that the number of atomic layers affects the surface energies [34] and also the surface stability is affected by the choice of which atomic layer is fixed [35]. In addition, the step construction of anatase (100) surface is expected to increase the strength of adsorption of metal atoms on this surface [36]. The energies of both relaxed and unrelaxed surfaces are calculated for slabs with different thicknesses from 2 to 8 atomic layers, and plotted in Fig. 3.2. The energies (E_{surf}) of them are calculated by using the

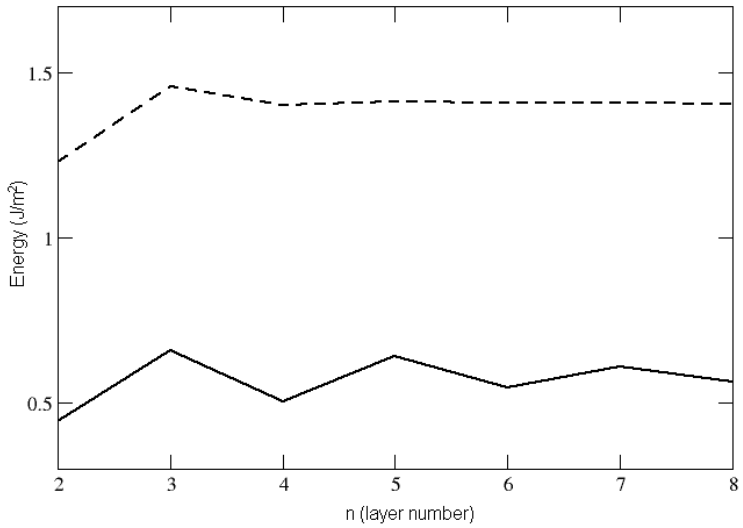

Figure 3.2: The surface energy (J/m^2) with respect to the number of Ti layers in the slab. Solid and dash lines represent the relaxed and unrelaxed slabs, respectively.

formula:

$$E_{\text{surf}} = \frac{1}{2A}(E_{\text{slab}} - nE_{\text{bulk}}) \tag{3.1}$$

where, E_{slab} and E_{bulk} are the total slab energies and the bulk anatase energies, respectively, n is the number of TiO_2 units within the slab, and A is the surface area. The factor of $1/2$ is due to the existence of two symmetrical surfaces for each slab. The energy values of those with odd number of layers are lower than those with the even number of atomic layers. However, the energy difference between slabs with odd and even numbers of atomic layers decreases as the thickness increases. The higher thickness is more stable and the surface energy converges. Thus, the slab modelling the surface have been chosen such that seven TiO_2 layers are distributed in fourteen TiO_2 molecular units in the slab. the fourth layer, which is in the middle of the slab, is fixed in to keep the slab as symmetric.

A 1×1 surface unit has two two-fold oxygen atoms (O2c) causing the edges of step-like part, two three-fold oxygen atoms (O3c) and two five-fold titanium

atoms (Ti5c) along the [001] direction (Fig. 3.1). The surface and the sixth layer of Ti and O atoms after relaxation alter their positions, between bond lengths of each other and angle values. The structure of the relaxed slab is shown in Fig. 3.3(a) and also their structural change values are given in the Table 3.1. Ti5c atoms (Ti20 and T21) and O2c atoms (O21 and O22) are relaxed inward, while O3c atoms (O20 and O23) are relaxed outward at the surface. At the sixth layer of slab atoms, Ti6c (Ti10 and Ti11) and O3c (O10 and O13) atoms are relaxed outward, while O3c (O11 and O12) atoms are relaxed inward. The bond length between Ti20 and O21 (similarly, Ti21 and O22) got shorter after relaxation and angle between Ti20–O21–Ti10 atoms is slightly increased by about 0.4°. Similarly, the bond of Ti20 and O10 got shorter, while the change of angle of 8.0° between O21–Ti20–O10. The relaxed structure of anatase (100) is similar to that of (101) surface in terms of the position of O2c atoms on the surface. The distance between two O2c atoms located at the step-like construction is larger than that of their unrelaxed surface positions because O2c atoms have moved opposite direction until their the most stable positions. When these results are compared with the work of Lazzeri *et al.* [37], some values which are slightly observed to be different can be observed. Different choices of vacuum regions or the tolerances for the atomic forces especially near the fixed atomic layer may cause such small disagreements.

E_{surf} is calculated to be 1.41 J/m^2 and 0.61 J/m^2 for unrelaxed surface and relaxed surface, respectively. In previous works, Lazzeri *et al.* calculated the surface energies as $E_{\text{surf}}^{\text{rel}} = 0.53$ and $E_{\text{surf}}^{\text{unrel}} = 1.59$ J/m^2 for six-layer anatase (100) slab by using GGA-PBE method [37,38] and their results for the same slab were found to be $E_{\text{surf}}^{\text{rel}} = 0.56$ and $E_{\text{surf}}^{\text{unrel}} = 1.44$ J/m^2 using GGA-PW91 method by Calatayud and Minot [35]. Our calculated energy values are nearly in agreement with these results. Finally, it can be said that the unrelaxed surface is less stable compared to the relaxed surface in terms of their surface energy values.

The indirect energy gap of anatase bulk is found to be ∼1.92 eV in electronic

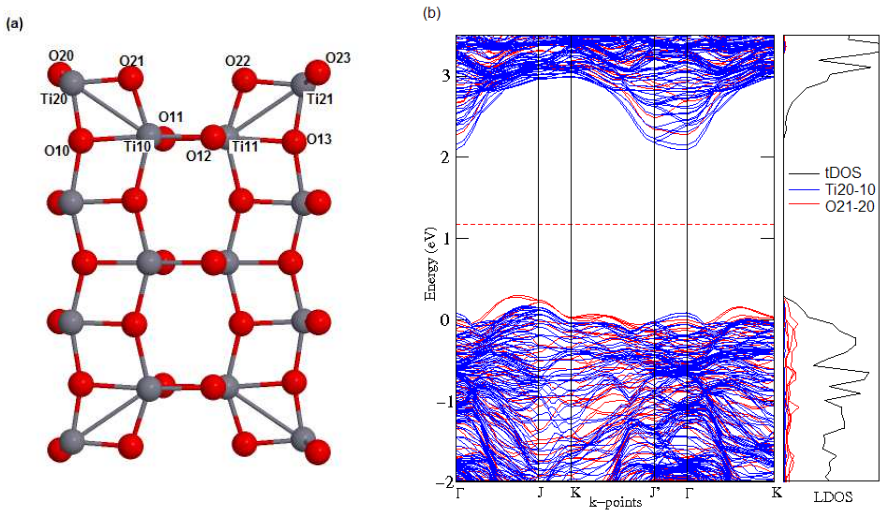

Figure 3.3: (a) Reconstructed (100) slab unit cell. (b) The band structure of the relaxed surface (red lines), bulk bands projected on the same surface Brillouin zone (blue lines) and the LDOS plots in the rightmost panel. Energies are measured with respect to the valence band top and the (red) dash line indicates the Fermi level.

band structure calculation. However, the experimental band gap is ∼3.2 eV at room temperature [39,40]. These values are apparently very different when they are compared to each other. The reason for that is the band gap calculations in solids is still problematic, because of the underestimation of the gap, an artifact of DFT. The surface electronic band structure (BS) and projected bulk electronic BS are represented by the red and blue lines, respectively, in Fig. 3.3(b). When surface and projected bulk band gaps are compared to each other, they are ∼1.96 eV and ∼1.90 eV, respectively. After relaxation, we observed that the bond lengths between Ti20–O21 and T21–O22 on the reconstructed surface are shorter than their bond lengths at the unrelaxed surface. It can be explained that unsaturated Ti–O atoms have 'dangling' bonds exposed to the vacuum. The reason of both the decrease of surface energy and states which come from VB are these dangling bonds. According to projected (local) density of state, O atom states are more populated in the VB which is mainly composed

Table 3.1: Change in structural parameters of anatase (100) surface upon relaxation. Atom labels are as defined in Fig. 3.3.

Displacement (Å)			Bond expansion		Angle (°)		
A	[001]	[100]	A–B	%	C–A–B	unrelaxed	relaxed
Ti10	−0.03	+0.15	A–O21	+3.6	O10–A–B	77.5	76.3
Ti11	+0.03	+0.15	A–O12	−0.5	O11–A–B	77.5	77.3
Ti20	−0.00	−0.11	A–O11	+7.1	O21–A–B	77.5	85.5
Ti21	+0.00	−0.11	A–O13	+7.1	O22–A–B	77.5	85.5
O10	−0.11	−0.03	A–Ti10	−6.0	Ti20–A–B	102.5	95.3
O11	+0.01	+0.06	A–Ti10	+0.5	Ti11–A–B	102.5	102.7
O12	−0.01	+0.06	A–Ti11	+0.5	Ti10–A–B	102.5	102.7
O13	+0.11	−0.03	A–Ti21	−0.6	Ti11–A–B	102.5	95.3
O20	+0.03	+0.18	A–Ti20	+1.5			
O21	−0.14	−0.01	A–Ti20	+8.0	Ti10–A–B	102.5	102.9
O22	+0.24	−0.01	A–Ti21	+8.0	Ti11–A–B	102.5	102.9
O23	−0.03	+0.18	A–Ti21	+1.5			

of Ti and O states, while Ti states are predominantly at the CB. The lowest energy band of unfilled states (CB minimum) is at Γ and the highest filled band (surface state) is along the $\overline{\Gamma J}$ direction.

3.2.2 Single gold adsorption

We have addressed the problem in two parts, the first part deal with a single Au atom adsorption and the other containing more than one atom adsorbed on the clean and unclean TiO_2 anatase (100) surfaces. By 'unclean' it is meant that the surface has other Au impurity atoms already adsorbed on it. In the first part four different adsorption models for a single Au atom adsorbed on the (1×1) cell of the clean surface have been considered. In the first model, a single Au atom is adsorbed on the two-fold coordinated surface oxygen atoms,

O2c. The highest adsorption energy is found for this model compared to the other single gold adsorption sites. In the second model, Au atom bonds weakly with only one of the O2c atoms on the surface. In the third model, single Au atom bonds with the five-fold surface Ti atom, Ti5c, so the properties of the interaction between Au and Ti atoms could be investigated. In the last model of this part, the single Au atom adsorbs between O2c and Ti5c atoms, where the interaction between Au and Ti atoms is more dominant compared to that of Au and O atoms. In the second part, the surface has a single Au atom in the beginnings, followed by the addition of the second, the third, and the fourth single Au atoms. In other words, the anatase (100) surface has an Au impurity atom adsorbed already in the site defined in model 1 having the strongest binding, and new Au impurities are to be adsorbed to this system, so that it will be a check for whether a mono atomic chain can be created with gold atoms on the surface. During all these processes, the dangling bonds on both top and bottom surfaces of the slab are synchronously saturated with Au single or multiple atoms without breaking the symmetry of the slab. On the other hand, when only the dangling bonds originated from O2c or Ti5c at the top surface are saturated with Au atom or atoms, surface bands coming from the dangling bonds of the bottom surface of the slab will still be in the gap. Thus, the slab covered with Au adsorbates should also be symmetrical. Additionally, the adsorption energy per Au atom E^{a} has been calculated as follows;

$$E^{\mathrm{a}} = (E_{\mathrm{TiO_2}} + nE_{\mathrm{Au}} - E_{\mathrm{TiO_2+nAu}})/n \ . \tag{3.2}$$

In this formula, $E_{\mathrm{TiO_2}}$, E_{Au}, and $E_{\mathrm{TiO_2+nAu}}$ are the total energies of the relaxed clean slab, free Au atom, and the relaxed slab+Au system. Here, n is the number of Au atoms adsorbed on the surface.

Au absorbed on the surface

The first model for the adsorption of a single Au atom on the surface, has a single Au atom adsorbed between two O2c oxygen atoms on the reconstructed

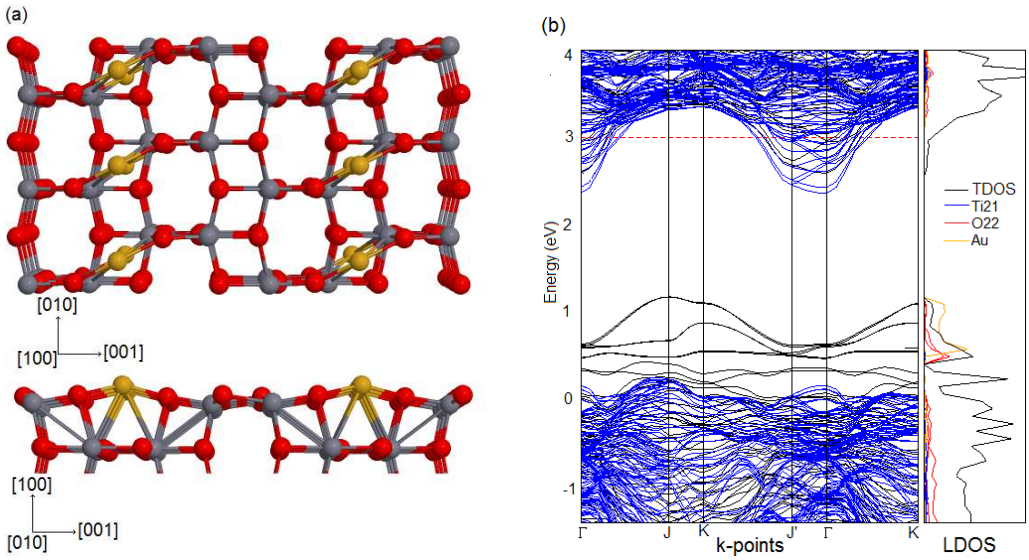

Figure 3.4: (a) The top and front views of the **single Au** atom adsorbed on anatase(100)-1×1 surface (model 1). (b) The electronic band structures of the combined Au–anatase system (black lines) and the projected bulk bands (blue lines), and the LDOS plots on the rightmost panel.

anatase (100) surface, Au(O,O), as shown in Fig 3.4(a). The distance between neighboring Au atoms which is determined by the surface periodicity is too large for a metallic chain to form for a comparison. The bond length of Au–Au changes between 2.88 Å for bulk structure and 2.54 Å for nanowire zigzag structure, but Au–Au distance was found to be 3.83 Å value in this model. The results for adsorption energy per Au atom, Fermi level, Au–O, Au–Ti, and Au–Au distances are listed in Table 3.2. For the most stable adsorption site, bond lengths of Au–O21 (alike Au–O22) and Au–Ti10 (alike Au–Ti11) are 2.06 Å and 3.02 Å, also the angles of O21–Au–T10 and T10–Au–Ti11 are 46.8° and 62.3°, respectively (The numbers which referred to the surface atoms were shown in Fig 3.3(a)). The Fermi energy was provided directly from the result of relaxation process and it was adapted to the scale of band structure graph. The highest adsorption energy has been found as 0.88 eV in this model which is compared to other adsorption models of single Au on the surface. This value is smaller than the adsorption energy value of 1.07 eV which was found by Gong *et*

al. [41], because their selected surface area (1×2 reconstruction) is larger than ours. The adsorption energy is affected by the concentration of metal atoms adsorbed on the surface [42]. In addition, their used calculation methods are different from us.

The three impurity states which originate from the *s*-orbital of Au [43] are higher in energy in the band structure (Fig. 3.4(b)). O atoms are dominant in the other four defect states that are closer to VB. All impurity states come from VB because O atoms are more reactive and stay near the VB according to the band structure of the bare surface and a single Au atom binds with two O atoms. The impurity states are doubly degenerate because there are two Au atoms symmetrically adsorbed on the top and bottom surfaces of the slab. Au impurity states are illustrated in projected (local) density of state (LDOS) plot with orange color, which is shown in the rightmost panel of Fig. 3.4(b). According to the LDOS plot, the *p*-orbitals for oxygen states, depicted in red lines are more reactive than the Ti states in the high energy levels of VB, although there are small contributions from Ti states. However, Ti states are dominantly in CB compared to Au and O states. Total density of state of the model is presented with black line in the plot. The band gap reduced from ∼1.96 eV for the clean surface to ∼1.41 eV due to Au impurity states. This model does not gain metallic character in terms of the band gap value. Minimum energy value for the CB is along $\overline{\mathrm{J'\Gamma}}$ direction. The reason for the energy difference of the occupied bands between *k*-points is the interaction between the adsorbed Au atoms which are located along the [010] direction from the surface period. The energy level of occupied bands have the highest value in the J point and the higher of them are sharply dispersed along $\overline{\Gamma\mathrm{J}}$ and $\overline{\mathrm{KJ'}}$ directions. Impurity states which have relatively lower energies are smoothly dispersed.

The second model in this part, single Au atom bonding with O2*c* atom located on the one edge of the step-like structure of the surface, Au(O), as shown in Fig. 3.5(a). Adsorption of the Au atom on the surface is weaker this time having a low adsorption energy value of ∼0.48 eV. The binding geometry

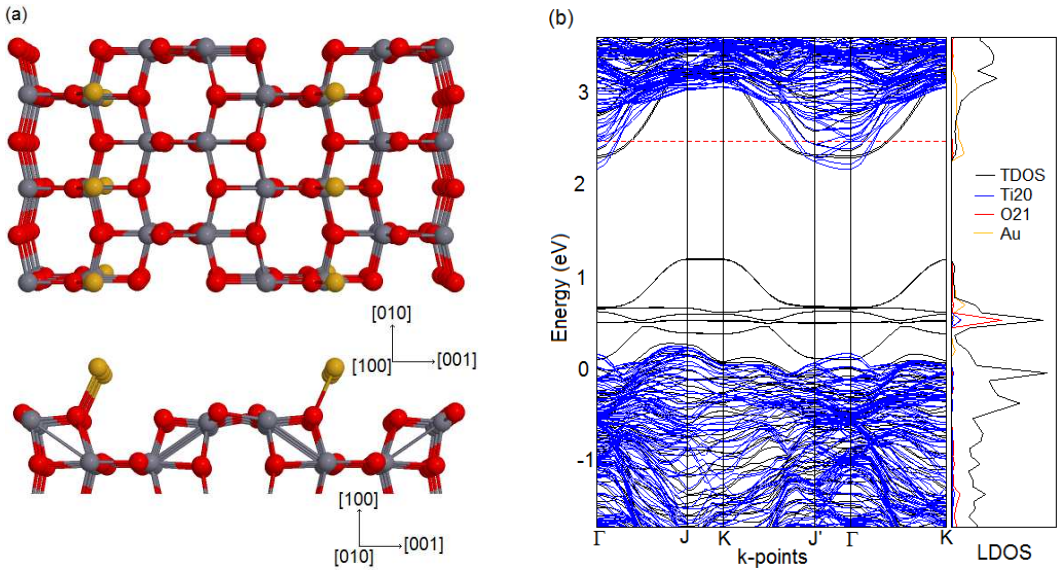

Figure 3.5: (a) The top and front views of the **single Au** atom adsorbed on O2*c* of anatase(100)-1×1 surface (model 2). (b) The electronic band structures of the combined Au–anatase system (black lines) and the projected bulk bands (blue lines), and the LDOS plots on the rightmost panel.

of this model is similar to a single Au atom adsorbed on the terrace oxygen sites of the anatase (101) surface. The bond lengths of Au–O21 atoms of ∼2.19 Å is bigger than that of Au(O,O) model. The angle values of Ti20–O21–Au and T10–O21–Au are found as 119.4° and 139.3°, respectively.

The energy band structure which is shown in Fig. 3.5(b) has six defect states at the energy gap. The five of them which are below the Fermi energy are occupied bands and one of them is above the CB minimum and empty. This empty defect state, the highest occupied band and the lowest of the six, the one right above the VB maximum are flat along one direction and dispersed as perfect cosine behavior in the in the direction normal to that. All these three bands are mainly of Au characters and they indicate a chain of gold atoms is formed and residing on the surface. Other states which are found between them have mainly of O and Ti contributions as shown in the LDOS plots. The energy gap is found to be ∼ 1.09 eV, which value is smaller than that of Au(O,O) model.

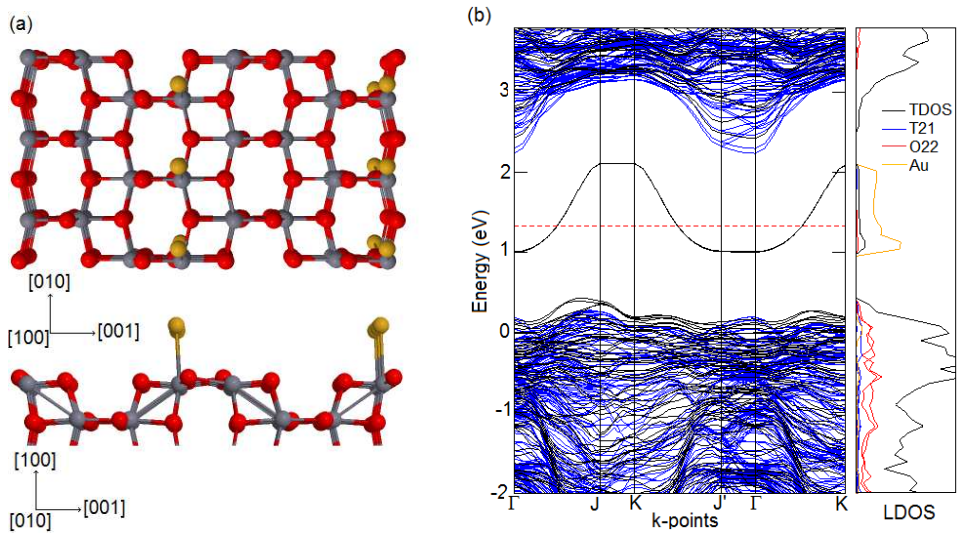

Figure 3.6: (a) The top and front views of the **single Au** adsorbed on Ti5*c* of anatase(100)-1×1 surface (model 3). (b) The electronic band structures of the combined Au–anatase system (black lines) and the projected bulk bands (blue lines), and the LDOS plots on the rightmost panel.

This model does not gain metallic character similarly to Au(O,O) model.

In the third model for this concentration, a single Au atom adsorbs on the unsaturated Ti21 atom which is located at the edge of the TiO_2 anatase (100) surface, Au(Ti), where the atomic structure is seen in Fig. 3.6(a). The calculational results are given in Table 3.2. Au has the weakest bond with Ti21 atom in this case because of the smallest adsorption energy of only 0.43 eV among all four models. Fermi energy is found nearly at 0.33 eV. At the most stable position, i.e. after the relaxation, Au–Ti21, Au–O20 ,and Au–O23 bond lengths are found to be 2.86 Å, 2.87 Å, and 3.23 Å, also the angle values of Au–T21–O20 and Au–Ti21–O23 are of 70.0° and 83.7°, respectively.

According to the electronic band structure which is shown in Fig. 3.6(b), there is only one impurity state which is in the middle of the gap and it is one dimensional as is also evident from the corresponding LDOS plots. Au is more dominant with a little mixing of Ti in this impurity band. Fermi energy almost halves this band causing a metallic surface due to the chains of gold atoms along

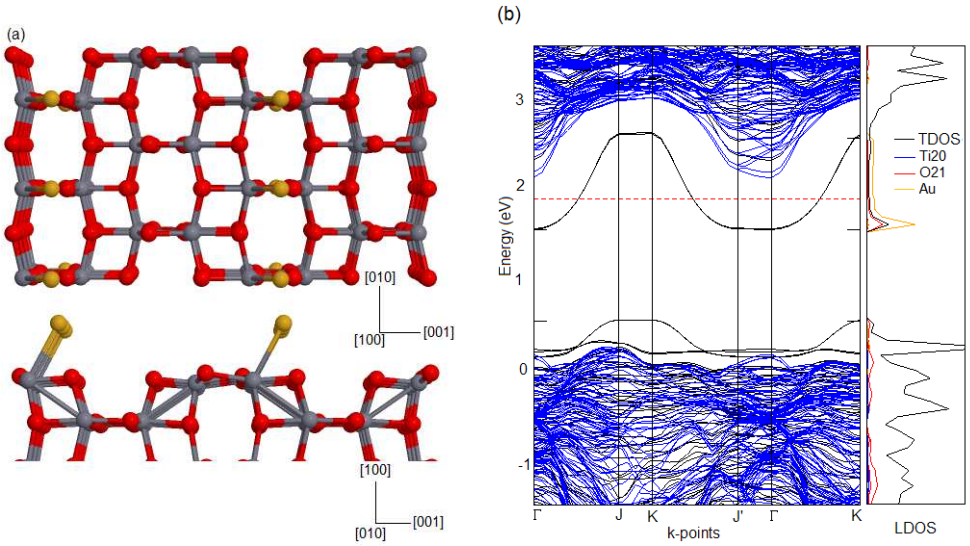

Figure 3.7: (a) The top and front views of the **single Au** adsorbed on Ti5*c* and O2*c* of anatase(100)-1×1 surface (model 4). (b) The electronic band structures of the combined Au–anatase system (black lines) and the projected bulk bands (blue lines), and the LDOS plots on the rightmost panel.

[010] direction. These chains can be considered as physisorbed on the anatase surface since the rest of the bands are very similar to that of the bare surface.

The last model in this part, a single Au atom adsorbing at a site close to Ti20 and O21 atoms which are located on the surface, labeled as Au(Ti,O), whose atomic structure is presented in Fig. 3.7(a), also the resulting parameters are given in Table 3.2. Adsorption of Au is slightly stronger than Au(Ti) model according to its adsorption energy of 0.51 eV. After complete relaxation the Au–Ti20 and Au–O21 bond lengths are found to be 2.81 Å and 2.43 Å, and also the angle values of Au–Ti20–O21, Au–O21–Ti20, and O21–Au–Ti20 are nearly equal to 58.3°, 80.1°, and 41.6°, respectively.

There are three impurity states originating from the state of Au impurity atom are seen in energy gap of this model, as shown in Fig. 3.7(b). One of them which is close to the CB originates from to interaction between Au and Ti20 atom . The Fermi energy level almost halves this energy band similar to the Au(Ti) case. In fact Au(Ti,O) is a case structurally and electronically right

between the Au(O) and Au(Ti) cases. The upper one-dimensional band is of Au and Ti character, whereas the one-dimensional state which is close to the valence band have O21 contributions since it is originated from the interaction between Au and O21 atoms at adsorption.

Effect of Au concentration

The first model in the second part of this section, the surface which has a single Au atom adsorbed on the two O2c atoms (Au(O,O)) is considered, because it was the strongest adsorption model supporting a single Au atom. A second single Au atom is adsorbed on the Ti5c atom which is labeled as Au-2(Ti), is shown in Fig. 3.8(a). Therefore, the metal concentration is increased in this model. After full relaxation, the bond lengths for Au–Ti21 and Au–O23 are found as 2.53 Å and 3.10 Å, respectively, and also the angle of Au–Ti21–O23 is of 86.7°. The adsorption energy of the added Au has been found to be 1.12 eV. (see Table 3.2). Some properties also change compared to applications of stable bare surface. In the first part, Au–Ti22 and Au–O23 distances were found to be 2.86 Å and 3.21 Å, respectively and also the adsorption energy of a single Au atom adsorbed on Ti21 was calculated to be 0.43 eV for the Au(Ti) model. In addition, a single Au atom adsorbed on an O 2c atom has the highest adsorption energy of 0.88 eV. According to these results, the adsorption energy of the second Au atom on the surface having an Au impurity already atom is higher than that of the bare surface applications. Also, the bond length of Au–Ti21 in the Au-2(Ti) model is considerably shorter than that of Au(Ti) model. As a result of that, one can see that the adsorption energy of Au is affected by the higher metal ad atom concentration on the surface. Moreover, the distances between two Au atoms on the surface and other neighbor Au1 and Au5 atoms are still too small for binding.

The defect state which is close to the conduction band is originated from the adsorbed second Au atom. The band gap of this model is found to be 0.14 eV which is smaller than the one in previous models. Thus, TiO_2 anatase

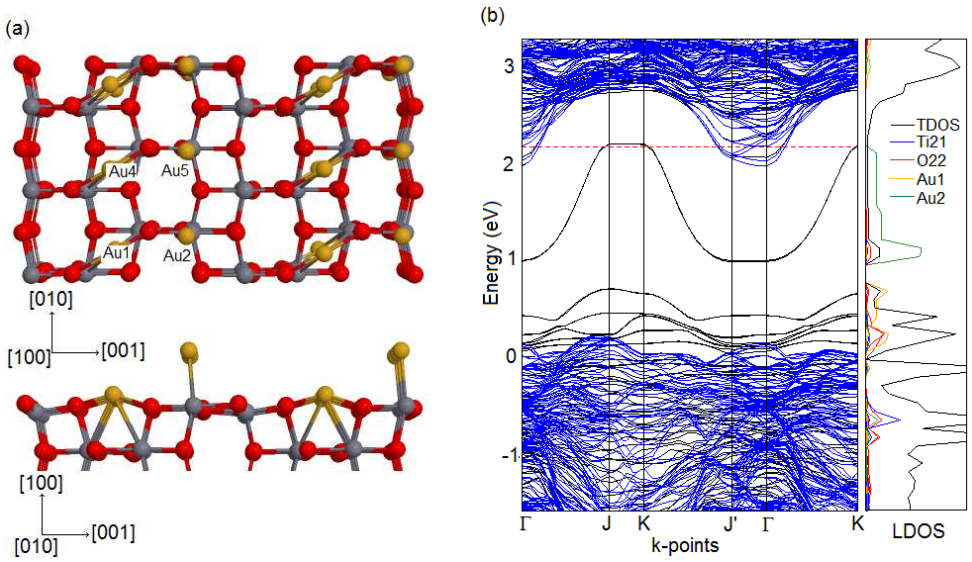

Figure 3.8: (a) The top and front views of the **second Au** atom adsorbed on Ti5*c* of anatase(100)-1×1 surface. (b) The electronic band structures of the combined Au–anatase system (black lines) and the projected bulk bands (blue lines), and the LDOS plots on the rightmost panel.

(100) surface which has two Au impurity atoms gains metallic property (Fig. 3.8(b)). LDOS graph apparently presents that band states are originated from Au energy states. Therefore, it could be deducted from this plot that the defect states which are close to the valence band top are originated from Au atom adsorbed on surface oxygen atoms and also the defect state close to conduction band comes form the Au atom bond ad to surface titanium atom. The band which is originated from Au adsorbed on Ti21 atom is completely occupied state different from that of Au(Ti) model although it is above the Fermi energy level along the $\overline{\text{JK}}$ direction which is unoccupied. This structure shows semi-metal character as its electronic property due to the overlap in energy of this band with that of the CB at different k-directions.

The second model in the part, a third single Au atom is adsorbed on Ti 5*c* where sit other edge of the surface (Au-c(Ti)). The atomic structure of this model is shown in Fig. 3.9(a). This way, the fills all the under coordinated (unsaturated) atoms on the surface. After the relaxation, Au–Ti20 and Au–O21

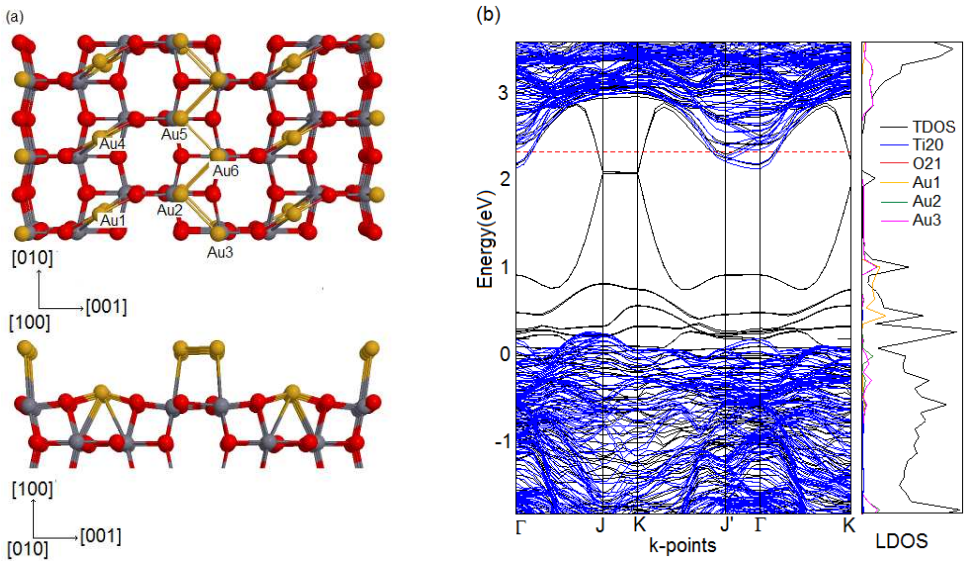

Figure 3.9: (a) The top and front views of the **third Au** atom adsorbed on Ti5*c* of anatase(100)-1×1 surface. (b) The electronic band structures of the combined Au–anatase system (black lines) and the projected bulk bands (blue lines), and the LDOS plots on the rightmost panel.

distance is nearly equal to 3.00 Åand 3.56 Å, and also the angles of Au–Ti20–O21 and Au–Ti20–O20 are found to be 90.6° and 84°, respectively. The highest adsorption energy for until all processes is calculated 2.06 eV (Table 3.2). The third single Au atom adsorbed on Ti20 bonds with other Au ad atom adsorbed on Ti21 in this model and they make monoatomic zigzag chain. The distance between Au3–Au2 is nearly equal to 2.66 Å and the bond length of Au3–Au5 is found as 2.67 Å dictated by the surface periodicity. The Au2–Au3–Au5 and Au3–Au5–Au6 have the same values which is equal to 92.1°. The most stable configuration is thus a zigzag chain of Au atoms described in this case.

The electronic band structure of this case is very different from other models due to interactions among several Au atoms. The band gap is covered with impurity states. The unoccupied energy state which comes from conduction band is degenerate with occupied state which has the highest energy value along the $\overline{\text{JK}}$ direction. As a result of this degeneracy, the electron occupancy of these bands are nearly equal to each other along the $\overline{\text{JK}}$ direction. This

Table 3.2: Calculated electronic and structural parameters: adsorption energy per Au atom, Fermi energy, Au–O, Au–Ti and Au–Au distances for each model. For labeling refer to Figs. 3.4–3.9.

Model	E^{a} (eV)	E_F (eV)	d_{Au-O} (Å)	d_{Au-Ti} (Å)	d_{Au-Au} (Å)
Au(O,O)	0.88	2.93	2.06(O22,O23)	3.02(Ti10,Ti11)	3.83
Au(O)	0.48	2.45	2.19(O21)	–	3.83
Au(Ti)	0.43	1.27	2.87(O20)	2.86(Ti21)	3.83
			3.23(O23)		
Au(Ti,O)	0.51	1.83	2.43(O21)	2.81(Ti20)	3.83
Au-2(Ti)	1.12	2.18	3.21(O20)	2.53(Ti21)	4.08(Au1)
			3.10(O23)		3.83(Au5)
Au-c(Ti)	2.06	2.22	3.56(O21)	3.00(Ti20)	2.66(Au2)
				2.94(Ti21)	2.67(Au5)

degenerate band mainly originating from Au–Au interactions. Because the state originated from Au–Ti interaction is unoccupied along this direction at the Au-2(Ti) model and this unoccupied state is filled by the charge density of the third single Au atom adsorbed in the Au-c(Ti) model. The density of these Au atoms is presented green and pink peak which mostly overlap in the LDOS plot (Fig. 3.9(b)). In addition, the single Au binding to two O $2c$ atoms is still gives defect states in the band gap close to VB, just like in model 1 (Au(O,O) case).

In the last model, a fourth single Au atom is tried further for adsorption between Au1 and Au4 atoms. But the four Au atoms interacting with each other caused the bonds of Au1–O21 (O22), Au2–T21, and Au3–Ti20 to be broken. Au atoms do not bind with surface atoms any longer and they construct cluster which contain four gold atoms at a higher distance from the surface.

The chemical properties of a material are usually described in terms of charge distribution among atoms or ions. In general, the two methods proposed by Mulliken and Bader charge analysis are used to describe the charge

Table 3.3: Bader charge analysis results for Au–TiO_2(100) anatase systems. For labeling refer to Figs. 3.4–3.9.

Model	O21	O22	O23	Ti11	Ti20	Ti21	Au1	Au2	Au3
clean	−1.26	−1.26	−1.37	+2.62	+2.64	+2.64			
Au(O,O)	−1.19	−1.19	−1.37	+2.55	+2.56	+2.56	+0.51		
Au(O)	−1.19	−1.25	−1.38	−	+2.58	+2.63	+0.16		
Au(Ti)	−1.24	−1.19	−1.34	+2.62	+2.63	+2.58	−0.03		
Au(Ti,O)	−1.18	−1.25	−	+2.61	+2.58	+2.63	+0.01		
Au-2(Ti)	−1.20	−1.19	−1.33	+2.62	+2.59	+2.50	+0.53	−0.42	
Au-c(Ti)	−1.19	−1.19	−1.34	+2.57	+2.56	+2.56	+0.52	−0.10	−0.15

distribution. Mulliken population charge method [44] is based on the electronic configuration of atom described as wave function. However, many calculations with the Mulliken method would lead to deceptive because it appointed all the electrons to on atom [45]. The second method, the Bader charge analysis, basically an approach that considers each atom defined as the electronic charge density rather around them than electron wave function. In principle, Bader used a partition of the physical space into regions which are divided by a two dimensional (2-D) surface with local zero-flux. The region divided by the surface is called Bader region in which the gradient of the electron density is a minimum perpendicular to the surface [45,46,47]. In this thesis, Bader analysis method is used for the description of the charge distribution.

The many types of bond of TiO_2 anatase has been analyzed using the Bader method in several works. The Ti–O bond is small and it involves charged cations Ti and polar anions O [48]. The ions of bulk anatase are calculated to be $Q_{\mathrm{Ti}} = +2.64e$, and $Q_{\mathrm{O}} = -1.32e$. These results are consistent with the work of Mete *et al.* where they found as $Q_{\mathrm{Ti}} = +2.66e$, and $Q_{\mathrm{O}} = -1.33e$ [49]. Charge distribution of the surface ions, Ti11 ion sitting at the sixth layer of the slab and Au ions are given Table 3.3. This Table does not involve charge distribution of ions of the bottom surface of the slab because their values are the

same with ions of the top surface. According to table, the differences between charge values of bulk and the surface ions differ only slightly. In the Au(O,O) model, Au ion has positive value due to charge transfer to O ions. The charge density of Au ion is the highest value in terms of magnitude compared to other single Au adsorption models. It can be said that Au strongly adsorbs on the two oxygen atoms as seen from charge values. This result is consistent with the results of adsorption energy results. In the Au(Ti) model, Au binds with the Ti atom has negative value. Au poorly adsorbs on Ti atom because of its small charge value.

The magnitude of the charge Au-2 ion in the Au-2(Ti) model is high and it is very close to the magnitude of the charge of Au-1 ions, whereas that of Au-1 in Au(Ti) model is very small. Au-2(Ti) seems to strongly with Ti atom in contrast to Au(Ti). Similarly, charge magnitudes of Au-2 and Au-3 ions in the Au-c(Ti) models are higher than Au ions in Au(Ti) model although its value is lower than that of Au-2 ions in the Au-2(Ti) model. Consequently, the metal concentration on the surface enhances the charge transfer. This is because the band gap of Au supported on the surface is narrowed compared to that of the bare surface and the charge transfer is mostly between Au and Ti atoms whose contribution is mostly to the CB. In the mono atomic gold chain case, Au atom seems to weakly bind with Ti atoms related to the lowest charge value of Au atoms. Au2 atom lost charge density due to interact with Au3 atoms.

3.2.3 Gold dimer (Au_2) adsorption

Three different adsorption models for stable gold dimer adsorption on the TiO_2 anatase (100) surface have been considered, as their atomic structures are shown in Figs. 3.10(a) to 3.12(a). They are, one of Au atoms in the dimer adsorbs on O22 only, adsorbs on Ti21 only, or adsorb on both O21 and Ti20 unsaturated surface atoms, respectively. The adsorption, cohesive and Fermi energies for

this structure were listed in Table 3.4. This time, we use the formula:

$$E^{a}_{\mathrm{Au_n}} = E_{\mathrm{TiO_2}} + E_{\mathrm{Au_n}} - E_{\mathrm{Au_n+TiO_2}} \tag{3.3}$$

to calculate the adsorption energy for both Au_2 and Au_3 clusters. This formula and the one used in the previous subsection differs such that this is the adsorption energy per gold cluster, whereas the formula for previous examples gives the adsorption energy per gold adatom. Here, n present number of atoms in the gold cluster. Cohesive or average adsorption energy per atom is calculated by using the adsorption energy formula in the previous subsection.

In the first model for this case, one of Au atoms in the dimer (Au1) binds to one of the unsaturated oxygen atoms (e.g., O22) located on the surface (labelled as model Au_2(O)). The bond length of Au1–O22 was found as ∼2.19 Å which is the same as that of a single Au adsorption model, Au(O). Au1–Au2 distance was found to be ∼2.64 Å which is longer than that of a free stable Au dimer of length ∼2.56 Å. The reason for this bond length difference between Au1–Au2 originate from the competing interactions between Au1–Au2 dimer atoms and Au_2 dimer with the surface. The angles of Au1–Au2–Au3, Au2–Au1–O22, and Au1–O22–Ti11 were found as 93.2°, 134°, and 143.2°, respectively. As a result, the family of gold atoms form a zigzag chain of Au_2 dimers.

The most stable configuration compared to other dimer adsorption models corresponds to the Au_2(O) model with adsorption energy of 1.05 eV. The average adsorption energy, 1.69 eV, of Au_2(O) is, as expected, higher than the single Au adsorption cases on the bare surface (Table 3.2) because of the strong interaction between Au1–Au2 metal atoms. On the other hand, the adsorption energy of Au-2(Ti) model in the previous section, which has the same number of Au atoms, is higher than that of the Au_2(O) model. Its Fermi energy is almost at the same level with that of Au(O,O).

The impurity states which is close to the VB originate from Au1–O(22) interaction, as shown in Fig 3.10(b). The density of this states is shown with orange peak in the LDOS graph. However, the other impurity states closer to CB mainly originate from the Au2 atom bound to Au1 dimer atom, as their

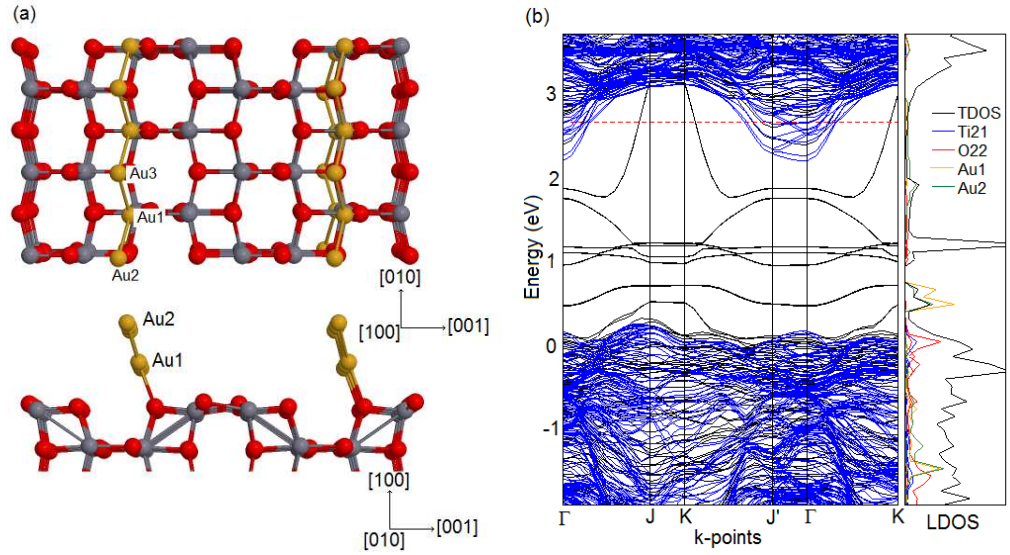

Figure 3.10: (a) The top and front views of the $\mathbf{Au_2}$ adsorbed on O2c of anatase(100)-1×1 surface. (b) The electronic band structures of the combined Au_2–anatase system (black lines) and the projected bulk bands (blue lines), and the LDOS plots on the rightmost panel.

Table 3.4: Calculated electronic and structural parameters: adsorption energy of Au_2, cohesive energy, Fermi energy, Au1–(O, Ti) and Au–Au distances for each model. For labeling refer to Figs. 3.11–3.13.

Model	E^{a} (eV)	E^{coh} (eV)	E_{F} (eV)	$d_{\mathrm{Au1-O,Ti}}$ (Å)	$d_{\mathrm{Au-Au}}$ (Å)
Au_2(O)	1.05	1.69	2.690.79	2.19(O22)	2.64(Au1–Au2)
					2.64(Au2–Au3)
Au_2(Ti)	0.83	1.58	2.34	2.83(Ti21)	2.63(Au1–Au2)
					2.63(Au1–Au3)
Au_2(Ti,O)	0.62	1.47	2.28	2.13(O21)	2.51(Au1–Au2)
				2.72(Ti20)	

density is presented in green lines in the LDOS graph. The defect state which is the closest to CB is unoccupied, above the Fermi energy level, along the $\overline{\mathrm{JK}}$ direction and occupied along other symmetry directions, therefore partially

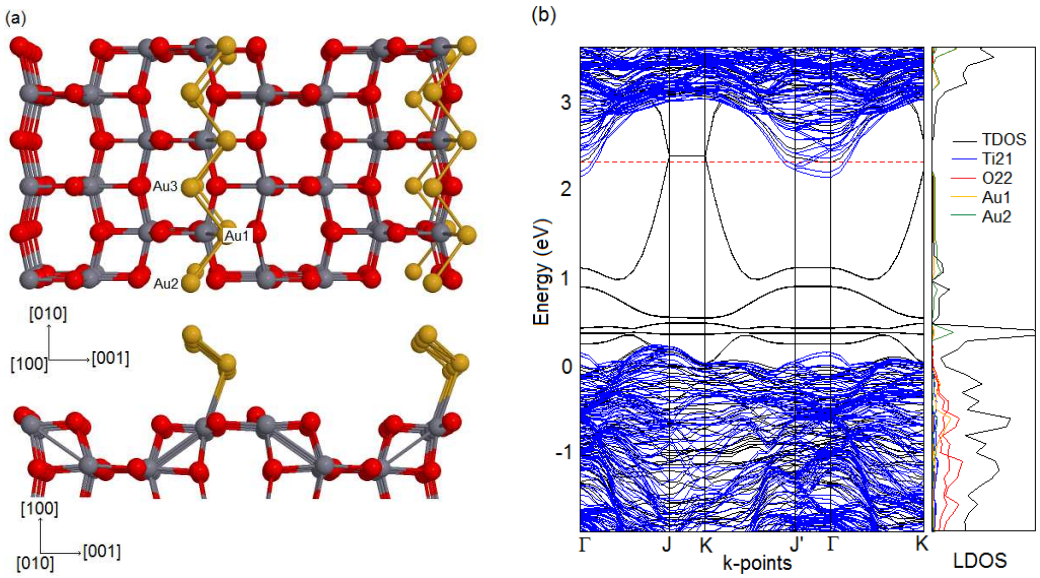

Figure 3.11: (a) The top and front views of the $\mathbf{Au}_2$ adsorbed on Ti5c of anatase(100)-1×1 surface. (b) The electronic band structures of the combined Au_2–anatase system (black lines) and the projected bulk bands (blue lines), and the LDOS plots on the rightmost panel.

occupied. Consequently, the band gap is nearly filled by defect states in the Au_2(O) model. This model shows metallic property.

In the second model for this subsection, one of the Au atoms in the gold dimer is adsorbed on Ti5c surface atom. The distance between Au1–Ti21 atoms was found to be 2.83 Å and it is slightly lower than that of a single Au with Ti 5c atom (2.86 Å) in the Au(Ti) model. The angles of Au2–Au1–Au3, Au2–Au1–Ti21, and Au1–Ti21–O22 are found as 93.8°, 102.8°, and 105.3°, respectively. The gold atoms are combined as a zigzag chain similar to the chain in the previous model, and the bond lengths of Au1–Au2 and Au2–Au3 in the chain are equal to the same value of 2.63 Å.

The adsorption energy is calculated as 0.83 eV and this value is lower than that of the Au_2(O) model. This result is similar to a previous observation that the adsorption energy of a single Au adsorption on Ti is lower than that of O atom. Cohesive energy is higher than the single Au atom adsorption cases on

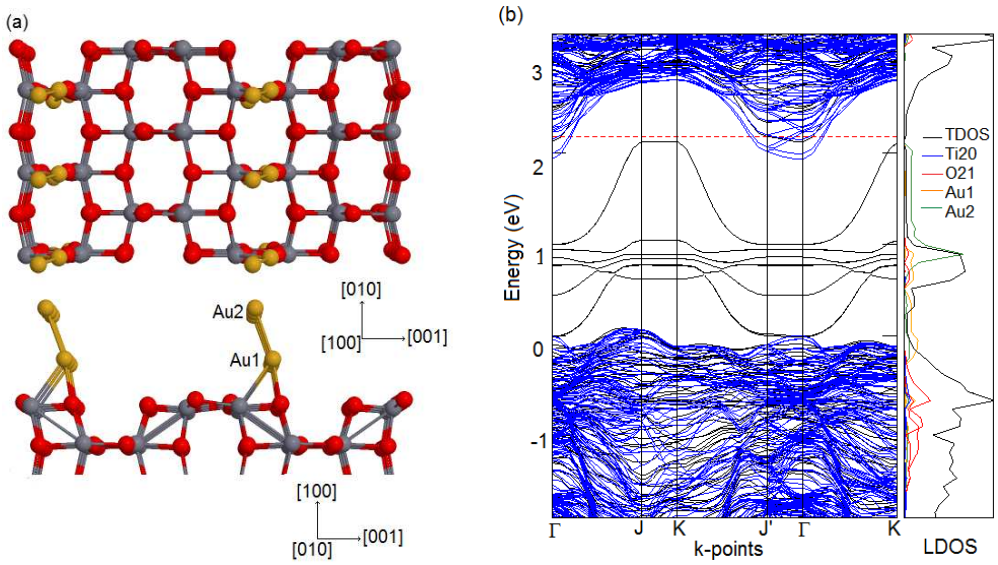

Figure 3.12: (a) The top and front views of the $\mathbf{Au_2}$ adsorbed on Ti5*c* and O2*c* of anatase(100)-1×1 surface. (b) The electronic band structures of the combined Au_2–anatase system (black lines) and the projected bulk bands (blue lines), and the LDOS plots on the rightmost panel.

the bare surface. However, it is lower than the cohesive energy for the Au_2(O) model. It can be said that Au–Au interaction strength is related to the strength of Au_2 adsorbed on the surface.

There are five defect states found in the energy gap, as shown in Fig. 3.11(b). They all are below the Fermi level and are occupied bands. However, the highest lying impurity state degenerates to a flat band along the $\overline{\text{JK}}$ direction with the unoccupied energy state coming from the CB, just above the Fermi level. Hence, it is also unoccupied in this direction. The defect states are predominantly of gold character as also seen in the LDOS plot of the same figure. Only one band which is closest to VB is mixed by the O22 states.

Last model, in this subsection, having one of the Au atoms in the gold dimer adsorbed on both unsaturated O21 and Ti20 atoms (Au_2(Ti,O)), which is shown in Fig. 3.12(a). The bond length of Au2–Ti20 was nearly equal to 2.72 Å, which is the lowest Au–Ti bond length among all cases except for that in the Au-2(Ti) model. Moreover, the Au1–O21 bond is equal to 2.13 Å, which is the shortest

among all Au dimer models. The dimer bond length (Au1–Au2) is equal to 2.53 Å, being the smallest one among all dimer models. The reason for this is because the Au atoms in this model can not bond to those Au atoms in the neighboring surface unit cells. The angles of Au1–O21–Ti20, Au1–Ti20–O21, and O21–Au1–Ti20 are 83.9°, 51.2°, and 44.9°, respectively.

The adsorption energy, being 0.62 eV, is the smallest of all the Au dimer structures. Therefore, the bond strength of dimer with the surface in the Au_2(Ti,O) model is the weakest among all dimer models according to their adsorption energy values, in spite of their shorter Au1–Ti20 and Au1–O21 bonds. The Fermi energy level is almost the same as that of the Au_2(Ti) model, whereas they are lower than that of the Au_2(O) model (see Table 3.4).

There are six impurity bands which are localized in the gap for the Au_2(Ti,O) model, as shown in Fig. 3.12(b). All of them are occupied states making the system metallic. Au2 is more localized in the region crowded with other less dispersed impurity bands, which is shown as a green peak in the LDOS plot. However, Au1 atom is predominantly localized in the lowest gap state. The highest gap state mostly of Au2 nature, on the other hand, is similar to those of Au–Ti interactions in the other adsorption models, having one-dimensional character. Unlike other Au dimer models, this band is not degenerate with CB because the Au2 atom does not bond with the gold atoms in the neighboring surface unit cells.

In the charge analysis for the Au_2(O) model, Au1 adsorbed on O2c looses more charge than that Au2 gains (see Table 3.5). The bond of Au1–O22 is the strongest among all three models due to highest charge density of Au1 in magnitude. The Au1–O22 interaction in the Au_2(O) is much smaller compared to Au(O,O) case in terms of their corresponding charge values, whereas it is just a little higher than that of the Au(O) model due to extra charge transfer to the dimer atoms. In the next model, Au1 bonding to Ti5c surface atom gains more charge density than the Au2 ion. However, the charge density of Au1 is considerably small magnitude as expected due to small charge transfer

Table 3.5: Bader charge analysis results for Au dimer on TiO_2(100) anatase system. For labeling refer to Figs. 3.11–3.13.

Model	O21	O22	Ti20	Ti21	Au1	Au2
clean	−1.26	−1.26	+2.64	+2.64		
Au_2(O)	−1.24	−1.21	+2.61	+2.58	+0.20	−0.06
Au_2(Ti)	−1.23	−1.20	+2.61	+2.58	−0.03	−0.00
Au_2(Ti,O)	−1.19	−1.21	+2.57	+2.58	+0.14	−0.11

between Au and Ti ions meaning the Au–Ti bond having covalent nature [50]. In the last model, Au2 ion has the highest charge density transferred among all gold dimer models which means the interaction between Au atoms is the strongest in this model. The reason for that is because the Au2 atom interacts only with Au1 atoms in the same unit cell as well as in the neighboring unit cell, thus forming a chain. The charge transfer of Au1 in this model is lower in magnitude than that in the Au_2(O) model, while it is higher than that in the Au_2(Ti) model, as expected. It is an interesting case since Au_2(O,Ti) has the weakest adsorption in all three Au_2 models. Therefore, the amount of charge transfer is generally smaller in Au–Ti bonds than in Au–O bonds.

3.2.4 Gold trimer (Au_3) adsorption

Two different models for stable gold trimer adsorption on the TiO_2 anatase (100) surface are considered, whose atomic structures are shown in Figs. 3.13(a) and 3.14(a). Two of the trimer-Au atoms bonding to the O22 and O21 atoms in one case, and one of the Au atoms bonds to both O22 and Ti21 unsaturated surface atoms, respectively. The adsorption, cohesive, and Fermi energies as well as the bond lengths of Au–O, Au–Ti, and Au–Au are listed in Table 3.6. Adsorption and cohesive energies were calculated by using same formulas in the gold dimer subsection.

In the first model for this case, two of the Au atoms (Au1 and Au2) in the

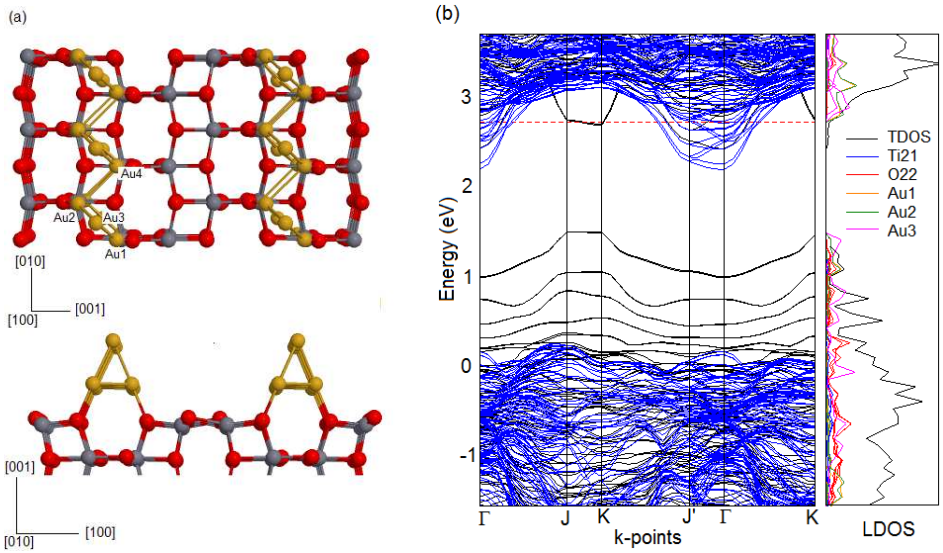

Figure 3.13: (a) The top and front views of the $\mathbf{Au}_3$ adsorbed on anatase(100)-1×1 surface. (b) The electronic band structures of the combined Au_3–anatase system (black lines) and the projected bulk bands (blue lines), and the LDOS plots on the rightmost panel.

planar cluster of triangular shape bind to unsaturated O2c atoms located on the surface (model Au_3(O,O)). The bond lengths Au–O21 and Au–O22 were found as 2.11 Å and 2.10 Å, respectively, which are lower than those in the Au(O) or the Au_2(O) models. Both Au3–Au1 and Au3–Au2 distances are found to be ∼2.64 Å which are shorter than length of Au1–Au2 to be ∼2.73 Å. The distance between two O2c atoms located on the step-like construction is slightly shortened by ∼0.09 Å with respect to their bare surface positions because of the interaction with Au_3 trimer adsorbed on them. The angles Au1–Au3–Au2, Au3–Au1–Au2, and Au1–Au2–Au3 are found to be 62.3°, 58.8° and 59.0° for the adsorbed trimer, respectively. Also, the angles O21–Au1–Au2 and O22–Au2–Au1 are found as 106.7° and 109.2°, respectively. Eventually, the family of gold atoms form a zigzag chain of Au_3 trimers and the bond length of Au2–Au4 in this chain is equal to ∼2.81 Å and the angle Au1–Au2–Au4 is found to be 87.6°.

The adsorption energy of the Au_3(O,O) model is calculated as ∼ 1.43 eV

Table 3.6: Calculated electronic and structural parameters: adsorption energy of Au_3, cohesive energy, Fermi energy, Au–O, and Au–Au distances for each model. For labeling refer to Figs. 3.15 and 3.16.

Model	E^{a} (eV)	E^{coh} (eV)	E_F (eV)	$d_{Au-(O,Ti)}$ (Å)	d_{Au-Au} (Å)
Au_3(O,O)	1.43	1.72	2.75	2.11(O21)	2.73(Au1–Au2)
				2.10(O22)	2.64(Au1;Au2–Au3)
					2.81(Au2–Au4)
Au_3(O,Ti)	0.79	1.50	2.39	2.11(O22)	2.77(Au1–Au2)
				2.90(Ti21)	2.58(Au1–Au3)
					2.73(Au2–Au3)

and this value is higher than that of the Au trimer model that follows. Cohesive energy is higher compared to the single Au atom models for the bare surface, and also higher compared to the Au dimer models. Consequently, the cohesive energy increases since the number of atoms in the gold cluster grows.

The band structure of this model is shown Fig. 3.13(b). Impurity states are all below the Fermi level and are occupied. The band gap is calculated as 0.93 eV. Maximum energy values of the impurity states is along the $\overline{JK}$ direction similar to the previous models. The impurity states are predominantly of gold character as also seen in the LDOS plot. They are located closer to VB due to Au–O interaction. The flat bands along JK of highest occupied state and the lowest unoccupied state are degenerate giving a zero gap in previous Au zigzag chain cases, however, because of the third Au atom of the trimer in this case these two flat bands are separated by a gap of about 1.50 eV due to Fermi level pinning of the upper band which is still unoccupied. However, this model shows metallic property due to the Au impurity states which are in the CB around Γ and J' points.

In the last model for this case, one of Au atoms in trimer is adsorbed on both unsaturated O22 and Ti21 surface atoms (Au_3(Ti,O)). The bond length of

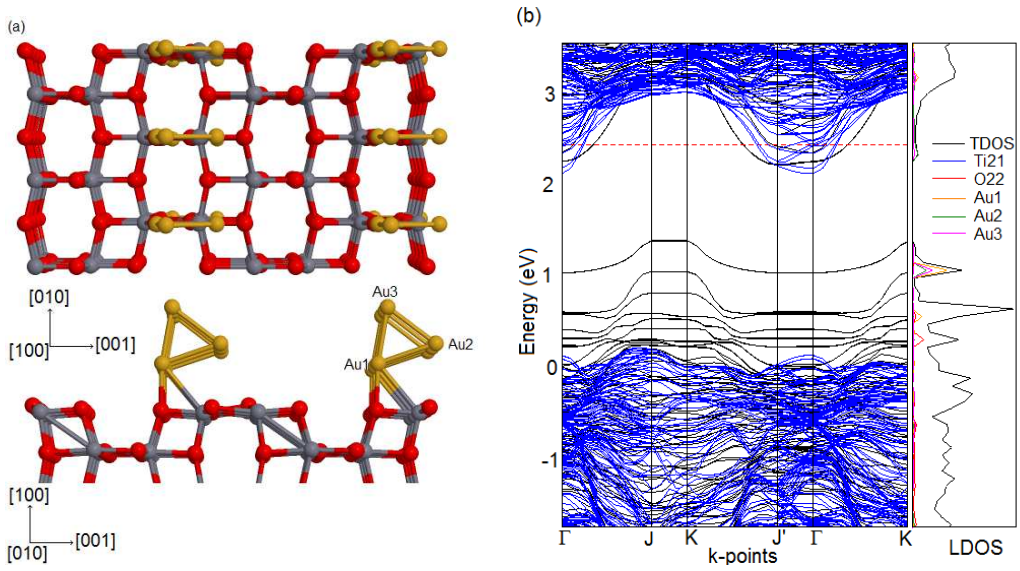

Figure 3.14: (a) The top and front views of the $\mathbf{Au}_3$ adsorbed on Ti5*c* and O2*c* of anatase(100)-1×1 surface. (b) The electronic band structures of the combined Au_3–anatase system (black lines) and the projected bulk bands (blue lines), and the LDOS plots on the rightmost panel.

Au1–O22 is the same as that of the Au_3(O,O) model and also the bond length of Au1–Ti21 is found as ∼2.90 Å. The bond lengths of Au atoms in the free trimer alter because of the interaction between trimer and the surface. As a result, Au3 atom is much closer to Au1 atom and Au2 atom is farther away from Au1 atom. The angles Au1–Au3–Au2, Au3–Au1–Au2, and Au1–Au2–Au3 are found as 62.8°, 61.2°, and 58.0° for the adsorbed trimer, respectively. On the other hand, the angles O22–Au1–Ti21, Ti21–O22–Au1, and O22–Ti21–Au1 are 41.4°, 92.1°, and 46.5°, respectively. The adsorption energy of this model is calculated to be ∼0.79 eV which is lower than that of the Au_3(O,O) model. Au atoms in this model weakly interact with those Au atoms in the neighboring surface unit cells but they can not bond to them.

The energy gap is found to be ∼0.83 eV according to the band structure shown in Fig. 3.14(b). The impurity states are predominantly coming from the Au1–O22 bonds. They are depicted in with orange and red lines in the LDOS plot. The defect state which is CB-derived is partially occupied, causing the

Table 3.7: Bader charge analysis results for Au_3 on $TiO_2(100)$ anatase system. For labeling refer to Figs. 3.15 and 3.16.

Model	Ti21	O21	O22	Au1	Au2	Au3
clean	+2.64	−1.26	−1.26			
Au_3^{free}				+0.08	−0.02	+0.00
Au_3(O,O)	+2.58	−1.23	−1.23	+0.23	+0.28	−0.08
Au_3(O,Ti)	+2.57	−1.22	−1.22	+0.30	−0.09	−0.07

system to have metallic property electronically.

In the charge analysis for the Au_3(O,O) model, both Au1 and Au2 ions loose charge due to interaction the two O2c atoms (see Table 3.7). Au3 ion gained negative charge transferred from both Au1 and Au2 ions. For the Au_3(O,Ti) model, O22–Au1 interaction is stronger than Ti21–Au1 as seen from the positive charge transferred to Au1, and moreover, Au2 and Au3 ions gain small amount of negative charge. Although the charge density of Au1 in Au_3(Ti,O) is higher than that in the Au_3(O,O) model, the charge magnitude of Au2 ion in the Au_3(Ti,O) is smaller than that in the Au_3(O,O) model. Therefore, the adsorption of Au atoms on the surface in the Au_3(O,O) model is stronger than Au_3(O,Ti).

CHAPTER 4

CONCLUSION

TiO_2 is generally used as a catalyst or a catalyst support and Au–TiO_2 is an active system for these applications. We have examined the structural and electronic properties of small Au_n ($n = 1-3$) clusters adsorbed on anatase (100)-1×1 reconstructed surface and these properties are investigated in terms of the Au concentrations per 1×1 unit cell area. The stable geometries for each metal and surface atoms have been obtained by relaxation to minimum total energy. According to our results, a single Au atom makes the strongest adsorption on two O2c of the surface with respect to other single-Au configurations. Also, Au dimer prefers to bind with O2c on the surface and the most stable configuration of Au trimer is adsorbed on two O2c surface atoms as well. Interactions between Au and Ti atoms are much weaker compared to that of Au and O atoms at the adsorption processes. However, Au–Ti becomes stronger as the second Au atom is adsorbed on the surface increasing the Au adatom concentration on the surface. The cohesive energy is increased when the number of Au atoms grow in the adsorbed metal cluster. The Au–Au bonds get stronger as the number of Au atoms increases.

The energy band gaps of structures with single Au adsorbates are decreased compared to that of the bare surface. The band gap of a single Au adsorbed on two O2c surface atoms is wider than that of other Au structures. The Au dimer structures gain metallic properties since the band gap of them is almost disappeared. The impurity states become degenerate in the case of metal chain

formation. The band gaps of Au-trimer cases are wider than that of Au-dimer models. The energy band gap of the case where two singe-Au atoms are adsorbed on the surface gets narrower than that of a single-Au structures, and also the gap for the tree single-Au structure is almost disappeared. It can be said that the system is gaining metallic property as the metal atom concentration on the surface increases. The impurity bands are closer to the valance band as adsorbed on O surface atoms and they are closer to the conduction band in relation to the interaction between Au and Ti atoms because the state populations of O and Ti atoms are high in the VB and CB, respectively. Fermi energy level is different for all cases but it is closer to the conduction band for the cases with relatively stronger bonding. This is because the occupied states are more energetic for the stronger adsorption.

REFERENCES

[1] U. Diebold, Surf. Sci. Rep. **48**, 53 (2003).

[2] M. R. Hoffmann, S. T. Martin, W. Choi, and D. W. Bahnemann, Chem. Rev. **95**, 69 (1995).

[3] M. Haruta, S. Tsubota, T. Kobayashi, H. Kageyama, M. J. Genet, and B. Delmon, J. Catal. **144**, 175 (1993).

[4] M. Haruta, Catal. Today **36**, 153 (1997).

[5] M. Valden, S. Pak, X. Lai, and D. W. Goodman, Catal. Lett. **56**, 7 (1998).

[6] M. Valden, X. Lai, and D. W. Goldman, Science **281**, 1647 (1998).

[7] A. G. Shastri, A. K. Datye, and J. Schwank, J. Catal. **87**, 265 (1984).

[8] G. C. Bond and D. T. Thompson, Catal. Rev. **41**, 319 (1999).

[9] A. Fujishima and K. Honda, Nature **238**, 38 (1972).

[10] A. L. Linsebigler, G. Lu, and J. T. Yates, Chem. Rev. **95**, 735 (1995).

[11] M. Grätzel, Nature **414**, 338 (2001).

[12] E. McFarland and J. Tang, Nature **421**, 616 (2003).

[13] A. Beltrán, L. Gracia, and J. Andrés, J. Phys. Chem. B **110**, 23417 (2006).

[14] G. Martra, Appl. Catal. A **200**, 275 (2000).

[15] A. Vittadini, A. Selloni, F. P. Rotzinger, and M. Grätzel, Phys. Rev. Lett. **81**, 2954 (1998).

[16] W. Hebenstrein, N. Ruzycki, G. S. Herman, Y. Gao, and U. Diebold, Phys. Rev. B **62**, 334 (2000).

[17] N. Ruzycki, G. S. Herman, L. A. Boatner, and U. Diebold, Surf. Sci. Lett. **529**, L239 (2003).

[18] A. Selloni, Nature **7**, 613 (2008).

[19] J. Kohanoff, "Electronic structure calculations for solids and molecules: theory and computational methods", Part 1, pp. 3–120, (Cambridge University Press, 2006).

[20] R. Martin, "Elctronic Structure: Basic Theory and Practical Methods", (Cambridge University Press, 2004).

[21] D. R. Hartree, Proc. Cambridge. Philos. Soc. **24**, 89 (1928).

[22] J. C. Slater, Phys. Rev. **35**, 210 (1930).

[23] L. H. Thomas, Proc. Chambridge Philos. Soc. **23**, **542** (1927).

[24] P. Hohenberg and W. Kohn, Phys. Rev. **136**, B864 (1964).

[25] W. Kohn and L. J. Sham, Phys. Rev. **140**, A1133 (1965).

[26] D. M. Ceperley and B. J. Alder, Phys. Rev. Lett. **45**, 566 (1980).

[27] J. P. Perdew, K. Burke, and M. Ernzerhof, Phys. Rev. Lett. **77**, 3865 (1996).

[28] D. Vanderbilt, Phys. Rev. B **41**, 7892 (1990).

[29] P. E. Blöchl, Phys. Rev. B **50**, 17953 (1994).

[30] G. Kresse and J. Halfner, J. Phys. Rev. B **48**, 13115 (1993).

[31] G. Kresse, M. Marsman, and J. Furthmüller, VASP, the Guide; (2009), http://cms.mpi.univie.ac.at/vasp/vasp/vasp.html.

[32] H. J. Monkhorst and J. D. Pack, Phys. Rev. B **13**, 5188 (1976).

[33] C. J. Howard, T. M. Sabine, and F. Dickson, Acta Crstallogr. Sect. B **47**, 462 (1991).

[34] F. Labat, P. Baranek, and C. Adamo, J. Chem. Theory Comput. **4**, 341 (2008).

[35] M. Calatayud and C. Minot, Surf. Sci. **552**, 169 (2004).

[36] X.-Q. Gong and A. Selloni, J. Catal. **249**, 134 (2007).

[37] M. Lazzeri, A. Vittadini, and A. Selloni, Phys. Rev. B **63**, 155403 (2001).

[38] M. Lazzeri, A. Vittadini, and A. Selloni, Phys. Rev. B **65**, 119901 (2002).

[39] S. P. Kowalczyk, F. R. McFeely, L. Levy, V. T. Gritsyna, and D. A. Shirley, Solid State Commun. **23**, 161 (1977).

[40] H. Tang, H. Berger, P. E. Schmid, F. Lévy, and G. Burri, Solid State Commun. **87**, 847 (1993).

[41] X.-Q. Gong, A. Selloni, O. Dulup, P. Jacobson, and U. Diebold, J. Am. Chem. Soc. **130**, 370 (2008).

[42] N. Lopez and J. K. Norskov, Surf. Sci. **515**, 175 (2002).

[43] A. Vittadini and A. Selloni, J. Chem. Phys. **117**, 353 (2002).

[44] R. S. Mulliken, J. Chem. Phys. **23**, 1833 (1955).

[45] E. Sanville, S. D. Kenny, R. Smith, and G. Henkelman, J. Comp. Chem. **28**, 899 (2007).

[46] G. Henkelman, A. Arnaldsson, and H. Jónsson, Comput. Mater. Sci. **36**, 354 (2006).

[47] W. Tang, E. Sanville, and G. Helkman, Condens. Matter **21**, 084204 (2009).

[48] M. Calatayud, P. Mori-Sánches, A. Beltrán, A. M. Pendás, E. Francisco, J. Andrés, and J. M. Recio, Phys. Rev. B **64**, 184113 (2001).

[49] E. Mete, D. Uner, O. Gülseren, and Ş. Ellialtıoğlu, Phys. Rev. B **79**, 125418 (2009).

[50] Y. Wang, G.S. Hwang, Surf. Sci. **542**, 72 (2003).